Progress in Fractional Differentiation and Applications
An International Journal

http://dx.doi.org/10.18576/pfda/120308

Adaptive LADM–Neural Remainder Correction for Atangana–Baleanu Fractional Hirota–Satsuma Coupled KdV Systems

Amin M. Elfeky[1], *Mohammad A. Tashtoush*[2,3], *Essa Melfi Aldosari*[4], *Mohamed Sayed Abdellatif*[5], *Adel S. Hussain*[6,7,8,*] *and Firas K. A. Al-Hamarneh*[9]

[1] Department of Mathematics, College of Science and Humanities, Prince Sattam Bin Abdulaziz University, Al-Kharj, Saudi Arabia
[2] Department of Basic Sciences, AL-Huson University College, AL-Balqa Applied University, Salt, Jordan
[3] Faculty of Education and Arts, Sohar University, Sohar, Oman
[4] Department of Curriculum and Instruction, College of Education in Al-Kharj, Prince Sattam Bin Abdulaziz University, Al-Kharj 11942, Saudi Arabia
[5] Department of Psychology, College of Education, Prince Sattam Bin Abdulaziz University, Al-Kharj 11942, Saudi Arabia
[6] IT Department, Amedi Technical Institutes, University of Duhok Polytechnic, Duhok, Iraq
[7] Department of Administrative and Financial Affairs, Faculty Division, Al-Iraqi University, Baghdad, Iraq
[8] Department of Computer Engineering, Al-Kitab University, Altun, Kupri, Kirkuk, Iraq
[9] Department of Allied Sciences, Faculty of Arts and Sciences, Al-Ahliyya Amman University, Amman 19328, Jordan

Received: 5 May. 2026, Revised: 8 Jun. 2026, Accepted: 27 Jun. 2026
Published online: 1 Jul. 2026

Abstract: The Atangana Baleanu fractional derivative is used to describe some memory effects by the GHS-Kdv system of nonlinear dispersive waves. However, it makes difficult to solve numerically this system. On the other hand, the Laplace-Adomian Decomposition Method (LADM), can be efficiently used to obtain a good approximation of the analytical solution of the GHS-Kdv system. But the precision obtained by this method depends of the number of decomposition terms that are considered. Moreover, even if we consider high numbers of terms, there is no guaranty that the precision will be better than the one obtained with lower numbers of terms. Therefore, to overcome these limitations, an adaptive Laplace-Adomian Neural Remainder Correction Framework has been developed. This new framework uses a truncated LADM approximation as an analytical base. It also uses a Multi-Output Neural Network trained only to predict the truncation remainder of the truncated LADM approximation. The proposed formulation allows to enforce exactly the initial conditions, and to keep the same nonlocal memory operator as in the problem statement, in the residual equation. It includes an adaptive LADM truncation criterion and an adaptive collocation based on residuals. Two test cases have been used to evaluate this new approach. They were compared with the analytical solution of the problem, and with numerical reference solutions. The results show that the efficiency of the neural corrections depend on the choice of the truncation order of LADM. For example, in a representative low-order case, the error was reduced from approximately $9.4x10^{-3}$ for pure LADM to $6.9x10^{-3}$ or the hybrid approximation, corresponding to an error-reduction factor of approximately 1.37. On the contrary, higher truncation orders can lead to greater correction errors, showing again how important is to select adaptively the number of decomposition terms.

Keywords: Atangana–Baleanu Caputo fractional derivative, generalized Hirota–Satsuma coupled KdV system, Laplace–Adomian decomposition method, adaptive LADM–neural network method, neural remainder correction, residual-based adaptive collocation, Sustainable Computational Innovation.

1 Introduction

Fractional calculus extends classical differentiation and integration to non-integer orders and provides a powerful mathematical framework for modeling systems with memory, hereditary behavior, and nonlocal temporal interactions. Such features arise naturally in viscoelastic materials, anomalous transport, complex fluids, plasma dynamics, and

* Corresponding author e-mail: adel.sufyan@dpu.edu.krd

© 2026 NSP
Natural Sciences Publishing Cor.

nonlinear optical media. Unlike integer-order models, fractional differential equations incorporate information from the previous evolution of the system and therefore offer additional flexibility in describing long-range temporal dependence and memory-controlled wave propagation [1,2,3,4,5].

Among nonlinear dispersive-wave models, the generalized Hirota-Satsuma (GHS) coupled Korteweg-de Vries (KdV) system has attracted considerable attention because of its ability to describe the interaction of multiple nonlinear wave fields. The model arises in applications related to shallow-water wave dynamics, ion-acoustic waves in plasma media, and nonlinear pulse propagation in optical systems [6,7,8,9]. Its mathematical structure combines third-order dispersion, nonlinear self-interaction, and coupling between multiple wave components, making the system considerably more challenging than the classical single-field KdV equation [10,11,12,13,14].

The incorporation of fractional temporal derivatives into the GHS-KdV system introduces an additional level of complexity. In particular, the Atangana-Baleanu derivative in the Caputo sense (AB-CFD) provides a nonlocal fractional operator characterized by a nonsingular Mittag-Leffler memory kernel [15,16,17]. In contrast to the classical Caputo and Riemann-Liouville operators, which involve singular power-law kernels, and the Caputo-Fabrizio derivative, which employs an exponentially decaying kernel, the AB-CFD combines nonsingular short-time behavior with persistent nonlocal memory. This property makes it particularly attractive for nonlinear wave systems in which the present evolution depends continuously on the previous temporal history [18,19,20].

For $0 < \theta \leq 1$, the fractional GHS coupled KdV system considered in this study is written as

$$ {}_0^{ABC}D_t^{\theta}\varphi(x,t) = \rho_1\varphi_{xxx}(x,t) - \rho_2\varphi(x,t)\varphi_x(x,t) + \rho_3(\psi(x,t)\phi(x,t))_x, \tag{1} $$

$$ {}_0^{ABC}D_t^{\theta}\psi(x,t) = -\sigma_1\psi_{xxx}(x,t) + \sigma_2\varphi(x,t)\psi_x(x,t), \tag{2} $$

and

$$ {}_0^{ABC}D_t^{\theta}\phi(x,t) = -\delta_1\phi_{xxx}(x,t) + \delta_2\varphi(x,t)\phi_x(x,t), \tag{3} $$

subject to the initial conditions

$$ \varphi(x,0) = \varphi_0(x),\ \psi(x,0) = \psi_0(x),\ \phi(x,0) = \phi_0(x). \tag{4} $$

Here, $\varphi(x,t), \psi(x,t)$, and $\phi(x,t)$ denote the interacting wave components, while $\rho_1, \rho_2, \rho_3, \sigma_1, \sigma_2, \delta_1$, and δ_2 control the strengths of the dispersive, nonlinear, and coupling mechanisms. The operator ${}_0^{ABC}D_t^{\theta}$ denotes the Atangana-Baleanu fractional derivative in the Caputo sense. As $\theta \to 1$, the corresponding classical GHS-KdV dynamics are recovered.

A variety of analytical, numerical, and semi-analytical methods have been proposed for fractional GHS-KdV-type systems. These include the Laplace residual power series method, modified Adomian decomposition techniques, homotopy-based transform methods, Legendre collocation procedures, pseudospectra schemes, and transform-based iterative approaches [21,22,23,24]. More recently, Laplace-enhanced Adomian decomposition and variational iteration methods have been formulated for the AB-CFD GHS-KdV system. Such approaches transform the fractional operator into a more tractable LaPlace domain representation while preserving the nonlinear structure of the governing equations. In particular, the Laplace Adomian decomposition method (LADM) represents the solution through recursively generated components and handles nonlinear terms using Adomian polynomials. The method avoids conventional perturbation and linearization assumptions and can provide high-accuracy low-order approximations. Despite these advantages, a fundamental limitation remains. In LADM, the approximate solution is obtained by truncating the decomposition series:

$$ \varphi_N^{LADM}(x,t) = \sum_{n=0}^{N}\varphi_n(x,t),\ \psi_N^{LADM}(x,t) = \sum_{n=0}^{N}\psi_n(x,t),\ \phi_N^{LADM}(x,t) = \sum_{n=0}^{N}\phi_n(x,t). \tag{5} $$

Increasing N generally improves the approximation; however, higher-order terms require increasingly complicated symbolic differentiation, nonlinear Adomian polynomial construction, Laplace transformation, and inverse transformation. Consequently, a trade-off arises between analytical accuracy and computational or symbolic complexity [25,26,27]. Furthermore, validation based primarily on the classical limit $\theta = 1$ does not completely quantify the unresolved approximation error in the genuinely fractional regime $0 < \theta < 1$. These observations motivate the development of a correction mechanism capable of preserving the analytical information produced by LADM while reducing the need for increasingly high decomposition orders. Neural networks provide a flexible alternative for approximating strongly nonlinear mappings and have recently become attractive tools for the numerical treatment of differential equations [28,29,30]. However, applying a neural network directly to a strongly nonlinear fractional partial differential equation requires the network to learn simultaneously the solution structure, nonlinear coupling, dispersion,

© 2026 NSP
Natural Sciences Publishing Cor.

initial data, and nonlocal temporal memory. Such a from-scratch formulation may lead to a difficult optimization problem and does not exploit the valuable analytical information already available from semi-analytical techniques such as LADM [31,32,33,34]. Therefore, rather than replacing LADM with a neural network, the present work adopts a hybrid analytical-neural strategy in which the two approaches perform complementary tasks. The central idea is to retain a low-order LADM approximation as an analytical backbone and employ a neural network only to approximate the unresolved remainder. Specifically, the proposed hybrid approximations are defined by

$$\widehat{\varphi}(x,t) = \varphi_N^{LADM}(x,t) + t\mathscr{N}_{\varphi}(x,t,\theta;\Theta), \tag{6}$$

$$\widehat{\psi}(x,t) = \psi_N^{LADM}(x,t) + t\mathscr{N}_{\psi}(x,t,\theta;\Theta), \tag{7}$$

and

$$\widehat{\phi}(x,t) = \phi_N^{LADM}(x,t) + t\mathscr{N}_{\phi}(x,t,\theta;\Theta) \tag{8}$$

where

$$\mathscr{N}_{\Theta}(x,t,\theta) = \big(\mathscr{N}_{\varphi}(x,t,\theta;\Theta), \mathscr{N}_{\psi}(x,t,\theta;\Theta), \mathscr{N}_{\phi}(x,t,\theta;\Theta)\big) \tag{9}$$

denotes a multi-output neural network with trainable parameters Θ. The LADM component captures the dominant analytical structure of the solution, whereas the neural component learns the unresolved remainder associated with finite truncation of the decomposition series. Multiplication of the neural correction by t guarantees that

$$\widehat{\varphi}(x,0) = \varphi_0(x),\ \widehat{\psi}(x,0) = \psi_0(x),\ \widehat{\phi}(x,0) = \phi_0(x), \tag{10}$$

provided that the underlying LADM approximation satisfies the prescribed initial conditions. Thus, the initial conditions are incorporated directly into the hybrid trial solution rather than being imposed only through penalty terms during neural-network training. The distinction between the proposed formulation and a conventional physics informed neural network is important. A standard neural approach approximates the complete unknown solution directly, whereas the proposed LADM-neural framework decomposes the solution conceptually as Consequently, the neural network does not need to reconstruct the dominant wave structure entirely from random initialization. Instead, it learns only the correction required to reduce the residual of the original fractional system. Substitution of the hybrid approximations into Eq. (1) and Eq. (3) leads to the fractional residuals

$$R_{\varphi} = {}_0^{ABC}D_t^{\theta}\widehat{\varphi} - \rho_1\widehat{\varphi}_{xxx} + \rho_2\widehat{\varphi}\widehat{\varphi}_x - \rho_3(\widehat{\psi}\widehat{\phi})_x, \tag{12}$$

$$R_{\psi} = {}_0^{ABC}D_t^{\theta}\widehat{\psi} + \sigma_1\widehat{\psi}_{xxx} - \sigma_2\widehat{\varphi}\widehat{\psi}_x, \tag{13}$$

and

$$R_{\phi} = {}_0^{ABC}D_t^{\theta}\widehat{\phi} + \delta_1\widehat{\phi}_{xxx} - \delta_2\widehat{\varphi}\widehat{\phi}_x. \tag{14}$$

The neural-network parameters Θ are optimized so that

$$R_{\varphi} \to 0,\ R_{\psi} \to 0,\ R_{\phi} \to 0 \tag{15}$$

throughout the computational domain. Importantly, the fractional operator is retained in its original Atangana-Baleanu form; therefore, the neural correction remains governed by the nonsingular Mittag-Leffler memory kernel rather than being replaced by an ordinary local time derivative. This formulation leads to the principal research gap addressed in the present study. Although LADM provides accurate semi-analytical approximations for fractional nonlinear wave systems, finite truncation leaves an unresolved remainder, while constructing higher-order Adomian components may substantially increase symbolic and computational complexity. Conversely, purely neural approaches do not exploit the analytical information already contained in low order decomposition solutions. A systematic framework that directly embeds a truncated LADM solution into a neural approximation and trains the network specifically to recover the unresolved fractional remainder is therefore required. The present work addresses this gap through an adaptive hybrid analytical neural correction strategy tailored to the AB-CFD GHS-KdV system. The results described above suggest a different research issue that can lead to new methods rather than new conclusions about previously developed hybrid models. Thus, the focus in this paper will be on using a truncated version of the LADM solution as the analytic base for correcting errors in the neural network solutions for only the portion of the model that was left out during the truncation process. Therefore, the focus of the current effort is on retaining the analytic structure that has been obtained through LADM (including the non-singularity of the Mittag-Leffler memory operator) as well as

© 2026 NSP
Natural Sciences Publishing Cor.

the exact enforcement of the initial conditions within the residual formulations. Also, the proposed approach combines the correction methodology with an adaptive truncation technique and residual-based collocation [35,36,37].

These complementary limitations motivate the proposed hybrid strategy. Rather than approximating the complete fractional solution with a neural network, the method retains a truncated LADM approximation as an analytical backbone and trains a multi-output neural network only on the unresolved remainder. In this way, the dominant wave structure already captured analytically is preserved, while the neural component is restricted to correcting the residual left by finite LADM truncation. The hybrid trial representation is constructed so that the prescribed initial conditions are satisfied exactly, and the original Atangana–Baleanu Caputo operator, including its nonsingular Mittag–Leffler memory kernel, is retained in the residual formulation [38,39,40,41,42]. The proposed framework therefore combines analytical structure, neural remainder correction, adaptive LADM truncation, and residual-based collocation within a single computational procedure. The main contributions of this study are summarized as follows:

1. A hybrid LADM-neural representation is developed for the Atangana-Baleanu fractional GHS coupled KdV system, in which truncated LADM solutions serve as analytical base functions and the neural network approximates only the unresolved remainder.
2. The initial conditions are incorporated exactly into the neural correction through a constrained trial representation, avoiding exclusive reliance on penalty-based enforcement.
3. The original AB-CFD operator, including its Mittag-Leffler memory kernel, is retained in the residual formulation so that the neural component remains consistent with the underlying fractional model.
4. An adaptive LADM truncation criterion is introduced to determine when further symbolic decomposition should be terminated and neural correction should become computationally preferable.
5. Residual-based adaptive collocation is incorporated to concentrate neural training points in regions where the hybrid approximation exhibits the largest fractional PDE mismatch.
6. The method is validated by comparing low-order LADM, the proposed LADM-neural approximation, and independent reference solutions through absolute errors, relative L^2 and L^∞ errors, fractional PDE residuals, and computational cost.
7. The influence of the fractional order θ on the wave dynamics and on the magnitude of the neural correction is investigated, providing a quantitative interpretation of the role of Atangana-Baleanu memory in the coupled nonlinear wave system.

The remainder of this paper is organized as follows. Section 2 introduces the mathematical preliminaries required for the proposed framework, including the Mittag–Leffler function, the Atangana–Baleanu fractional derivative in the Caputo sense, the Laplace transform, and the neural-network representation. Section 3 develops the proposed adaptive LADM–NN methodology, beginning with the LADM analytical backbone and proceeding to the adaptive truncation criterion, neural approximation of the unresolved LADM remainder, residual-driven correction equations, and the evaluation of the Atangana–Baleanu derivative of the neural correction. Section 4 describes the numerical experimental design, including the two benchmark problems, validation strategy in the genuinely fractional regime, adaptive LADM–NN evaluation protocol, and the error and performance measures used in the numerical assessment. Section 5 presents and discusses the numerical results, with particular emphasis on the accuracy of the hybrid approximation, the influence of the LADM truncation order and fractional order, the contribution of the neural remainder, residual-based adaptive collocation, computational efficiency, and comparisons with independent reference and previously published solutions. Finally, Section 6 summarizes the principal findings of the study and outlines directions for future research.

2 Mathematical Preliminaries

This section summarizes the mathematical tools required for the development of the proposed adaptive LADM-neural network framework. Particular attention is given to the Mittag-Leffler function, the Atangana-Baleanu fractional derivative in the Caputo sense, its Laplace-transform representation, and the neural-network correction used later in the hybrid approximation.

Definition 1. [14] For $\alpha > 0$ and $\beta > 0$, the two-parameter Mittag-Leffler function is defined by

$$E_{\alpha,\beta}(z) = \sum_{k=0}^{\infty} \frac{z^k}{\Gamma(\alpha k+\beta)}, \; z \in C. \tag{16}$$

The one-parameter Mittag-Leffler function is obtained by setting $\beta = 1$,

$$E_{\alpha}(z) = E_{\alpha,1}(z) = \sum_{k=0}^{\infty} \frac{z^k}{\Gamma(\alpha k+1)}. \tag{17}$$

In particular,

© 2026 NSP
Natural Sciences Publishing Cor.

$$E_1(z) = e^z \tag{18}$$

so that the Mittag-Leffler function may be regarded as a natural fractional generalization of the exponential function.

Definition 2. Let $F(x,t)$ be sufficiently differentiable with respect to t, and let $0 < \theta < 1$. The Atangana-Baleanu fractional derivative in the Caputo sense is defined by

$$ {}_0^{ABC}D_t^\theta F(x,t) = \frac{M(\theta)}{1-\theta}\int_0^t \frac{\partial F(x,s)}{\partial s} E_\theta\left(-\frac{\theta}{1-\theta}(t-s)^\theta\right) ds \tag{19}$$

where

$$M(\theta) = 1-\theta+\frac{\theta}{\Gamma(\theta)},\ M(0) = M(1) = 1. \tag{20}$$

The kernel is nonsingular and retains a Mittag-Leffler type temporal memory. This property is particularly important in the present work because the neural correction introduced later must preserve the same nonlocal memory structure as the original fractional GHS-KdV model. For a piecewise continuous function $F(x,t)$ of exponential order, the Laplace transform with respect to t is defined by:

$$\mathscr{L}_t\{F(x,t)\} = \widetilde{F}(x,s) = \int_0^\infty F(x,t)e^{-st}dt \tag{21}$$

Whenever the inverse exists, it is represented by the Bromwich integral

$$F(x,t) = \mathscr{L}_t^{-1}\{\widetilde{F}(x,s)\} = \frac{1}{2\pi i}\int_{c-i\infty}^{c+i\infty}\widetilde{F}(x,s)e^{st}ds \tag{22}$$

where c is chosen to the right of the singularities of $\widetilde{F}(x,s)$. The Laplace transform of the AB-Caputo derivative is given by

$$\mathscr{L}_t\left\{{}_0^{ABC}D_t^\theta F(x,t)\right\} = \frac{M(\theta)}{1-\theta}\frac{s^\theta\widetilde{F}(x,s)-s^{\theta-1}F(x,0)}{s^\theta+\theta 1-\theta}. \tag{23}$$

Equation Laplace to the LADM construction because it converts Henon local fracti for convenience, define

$$\omega_\theta(s) = \frac{\theta+(1-\theta)s^\theta}{M(\theta)s^\theta}, \tag{24}$$

which will be used later to simplify the recursive LADM formulas.

Definition 3. To complement the truncated LADM approximation, we introduce a multioutput feedforward neural network

$$\mathscr{N}_\Theta(x,t,\theta) = \mathscr{N}_\varphi(x,t,\theta;\Theta)\mathscr{N}_\psi(x,t,\theta;\Theta)\mathscr{N}_\phi(x,t,\theta;\Theta), \tag{25}$$

where Θ denotes the collection of trainable weights and biases. For a feedforward network with L hidden layers, the internal representation may be written recursively as

$$\mathbf{z}^{(0)} = xt\theta,\ \mathbf{z}^{(\updownarrow)} = \sigma\left(W^{(\updownarrow)}\mathbf{z}^{(\updownarrow-1)}+\mathbf{b}^{(\updownarrow)}\right),\ \updownarrow = 1,\ldots,L, \tag{26}$$

and

$$\mathscr{N}_\Theta = W^{(L+1)}\mathbf{z}^{(L)}+\mathbf{b}^{(L+1)}, \tag{27}$$

where σ denotes a sufficiently smooth activation function. In the proposed method, the neural network does not approximate the complete solution directly. Instead, it approximates the unresolved remainder of a finite LADM expansion. Thus, the hybrid approximation takes the general form

$$\widehat{\mathbf{U}}(x,t) = \mathbf{U}_N^{LADM}(x,t)+t\mathscr{N}_\Theta(x,t,\theta), \tag{28}$$

where

$$\mathbf{U}_N^{LADM} = \varphi_N^{LADM}\psi_N^{LADM}\phi_N^{LADM}. \tag{29}$$

The factor t ensures that the neural correction vanishes at the initial time. Consequently, if the LADM component satisfies the prescribed initial conditions, then

$$\widehat{\mathbf{U}}(x,0) = \mathbf{U}_0(x), \tag{30}$$

independently of the trainable neural-network parameters. The spatial derivatives required by the GHS-KdV operator, including first and third-order derivatives, are evaluated through automatic differentiation of the neural-network component. In contrast, the Atangana-Baleanu temporal derivative is evaluated using its original Mittag-Leffler memory representation in Eq. ABCFD; hence, the nonlocal fractional structure is preserved within the hybrid model.

© 2026 NSP
Natural Sciences Publishing Cor.

3 Proposed Adaptive LADM-Neural Network Method

This section develops the proposed adaptive hybrid Laplace-Adomian neural network (LADM-NN) framework for the Atangana-Baleanu fractional generalized Hirota-Satsuma coupled KdV system. The central principle is to use a low-order LADM approximation as an analytical backbone and to employ a neural network only for approximating the unresolved truncation remainder. Unlike a conventional neural approach, the proposed method does not require the neural network to reconstruct the complete solution from scratch. Instead, the neural component is driven by the residual left by a finite LADM expansion.

3.1 LADM Analytical Backbone

Consider the fractional GHS-KdV system

$$\begin{aligned}
{}_0^{ABC}D_t^{\theta}\varphi &= \rho_1\varphi_{xxx} - \rho_2\varphi\varphi_x + \rho_3(\psi\phi)_x,\\
{}_0^{ABC}D_t^{\theta}\psi &= -\sigma_1\psi_{xxx} + \sigma_2\varphi\psi_x,\\
{}_0^{ABC}D_t^{\theta}\phi &= -\delta_1\phi_{xxx} + \delta_2\varphi\phi_x,
\end{aligned}$$

subject to

$$\varphi(x,0) = \varphi_0(x),\ \psi(x,0) = \psi_0(x),\ \phi(x,0) = \phi_0(x). \tag{31}$$

Using the Laplace-transform representation of the AB-Caputo derivative introduced in Section ??, define

$$\omega_\theta(s) = \tfrac{(1-\theta)s^\theta+\theta}{M(\theta)s^\theta}. \tag{32}$$

Applying the Laplace transform with respect to t and subsequently taking the inverse transform gives

$$\begin{aligned}
\varphi(x,t) &= \varphi_0(x) + \mathscr{L}_t^{-1}\left\{\omega_\theta(s)\mathscr{L}_t\left[\rho_1\varphi_{xxx} - \rho_2\varphi\varphi_x + \rho_3(\psi\phi)_x\right]\right\},\\
\psi(x,t) &= \psi_0(x) + \mathscr{L}_t^{-1}\left\{\omega_\theta(s)\mathscr{L}_t\left[-\sigma_1\psi_{xxx} + \sigma_2\varphi\psi_x\right]\right\},\\
\phi(x,t) &= \phi_0(x) + \mathscr{L}_t^{-1}\left\{\omega_\theta(s)\mathscr{L}_t\left[-\delta_1\phi_{xxx} + \delta_2\varphi\phi_x\right]\right\}.
\end{aligned}$$

The LADM represents the three solution components as

$$\varphi = \textstyle\sum_{n=0}^{\infty}\varphi_n,\ \psi = \sum_{n=0}^{\infty}\psi_n,\ \phi = \sum_{n=0}^{\infty}\phi_n. \tag{33}$$

For the nonlinear terms, we introduce

$$\begin{aligned}
\varphi\varphi_x &= \sum_{n=0}^{\infty}\Xi_n, & \psi_x\phi &= \sum_{n=0}^{\infty}P_n,\\
\psi\phi_x &= \sum_{n=0}^{\infty}K_n, & \varphi\psi_x &= \sum_{n=0}^{\infty}\Upsilon_n, & \varphi\phi_x &= \sum_{n=0}^{\infty}\Omega_n.
\end{aligned} \tag{34}$$

Since all nonlinearities appearing in the present system are bilinear, the corresponding Adomian components can be written directly in convolution form:

$$\begin{aligned}
\Xi_n &= \sum_{j=0}^{n}\varphi_j\frac{\partial\varphi_{n-j}}{\partial x}, & P_n &= \sum_{j=0}^{n}\frac{\partial\psi_j}{\partial x}\phi_{n-j}, & K_n &= \sum_{j=0}^{n}\psi_j\frac{\partial\phi_{n-j}}{\partial x},\\
\Upsilon_n &= \sum_{j=0}^{n}\varphi_j\frac{\partial\psi_{n-j}}{\partial x}, & \Omega_n &= \sum_{j=0}^{n}\varphi_j\frac{\partial\phi_{n-j}}{\partial x}.
\end{aligned}$$

This representation is equivalent to the standard Adomian-polynomial construction but is more convenient for the bilinear nonlinearities of the GHS-KdV system. The initial LADM components are

$$\varphi_0(x,t) = \varphi_0(x),\ \psi_0(x,t) = \psi_0(x),\ \phi_0(x,t) = \phi_0(x). \tag{35}$$

© 2026 NSP
Natural Sciences Publishing Cor.

For $n \geq 0$, the recursive components are generated by

$$\begin{aligned}
\varphi_{n+1} &= \mathscr{L}_t^{-1}\left\{\omega_\theta(s)\mathscr{L}_t\left[\rho_1(\varphi_n)_{xxx} - \rho_2\Xi_n + \rho_3(P_n + K_n)\right]\right\},\\
\psi_{n+1} &= \mathscr{L}_t^{-1}\left\{\omega_\theta(s)\mathscr{L}_t\left[-\sigma_1(\psi_n)_{xxx} + \sigma_2\Upsilon_n\right]\right\},\\
\phi_{n+1} &= \mathscr{L}_t^{-1}\left\{\omega_\theta(s)\mathscr{L}_t\left[-\delta_1(\phi_n)_{xxx} + \delta_2\Omega_n\right]\right\}.
\end{aligned}$$

After N decomposition components, the finite LADM approximation is defined by

$$\mathbf{U}_N^{LADM}(x,t) = \left(\varphi_N^{LADM}, \psi_N^{LADM}, \phi_N^{LADM}\right) = \left(\sum_{n=0}^{N}\varphi_n, \sum_{n=0}^{N}\psi_n, \sum_{n=0}^{N}\phi_n\right). \tag{36}$$

If the infinite decomposition series converges in an appropriate function space, its limit provides a solution of the corresponding integral formulation. In the present work, however, no assumption of exactness is made for a finite truncation; instead, the unresolved remainder is quantified and subsequently corrected by the neural component.

3.2 Adaptive Truncation of the LADM Expansion

A central objective of the proposed framework is to avoid computing unnecessarily high-order Adomian components. To monitor the variation between successive truncated LADM approximations, we define

$$\eta_N = \frac{\left\|\mathbf{U}_N^{LADM} - \mathbf{U}_{N-1}^{LADM}\right\|_X}{\left\|\mathbf{U}_N^{LADM}\right\|_X + \varepsilon}, \tag{37}$$

where $\varepsilon > 0$ is a small regularization constant and $\|\cdot\|_X$ denotes a prescribed discrete or continuous solution norm. In addition, the residual of the truncated LADM approximation is defined as

$$\mathbf{R}_N^{LADM} = \left(R_{\varphi,N}^{LADM}, R_{\psi,N}^{LADM}, R_{\phi,N}^{LADM}\right) = \mathscr{F}\left(\mathbf{U}_N^{LADM}\right), \tag{38}$$

where $\mathscr{F}$ denotes the original fractional GHS-KdV operator. The normalized residual indicator is

$$\mathscr{E}_N^R = \frac{\left\|\mathbf{R}_N^{LADM}\right\|_Y}{\mathscr{S}_N + \varepsilon}, \tag{39}$$

where $\mathscr{S}_N$ is a characteristic magnitude of the terms appearing in the governing equations. If

$$\mathscr{E}_N^R \leq \tau_R, \tag{40}$$

the truncated LADM approximation is considered sufficiently accurate for the prescribed tolerance.

Otherwise, if

$$\eta_N \leq \tau_A \text{ or } N = N_{\max}, \tag{41}$$

then the expansion is terminated, the order $N^* = N$ is selected, and the neural remainder correction of Section 3.3 is activated. If neither condition (40), condition (41) nor the safeguard holds, N is increased by one and the next LADM component is computed. The test starts at $N = 1$, so that at least one time-dependent component is retained. The safeguard is required because, for the present dispersive system, the n-th Adomian component contains spatial derivatives of order $3n$ of the initial data; the truncated series therefore behaves asymptotically, and beyond a certain order the residual grows even when the increments η_N are still decreasing.

Definition of the Norms. All indicators are evaluated on the discrete space–time set $\Omega_h = \{x_i\} \times \{t_j\}$, with $x_i = -20 + 40i/N_x$ $(i = 0, \ldots, N_x - 1,\ N_x = 512)$ and $t_j = jT/40$ $(j = 1, \ldots, 40,\ T = 0.2)$. For a vector field $\mathbf{V} = (V_\varphi, V_\psi, V_\phi)$ defined on Ω_h, we set

$$\|\mathbf{V}\|_X = \left(\Delta x \Delta t \sum_{i,j}\left[V_\varphi^2(x_i,t_j) + V_\psi^2(x_i,t_j) + V_\phi^2(x_i,t_j)\right]\right)^{1/2}.$$

Threshold Values. Throughout the numerical experiments we use $\tau_R = 10^{-3}$, $\tau_A = 10^{-2}$, $N_{\max} = 4$ and $\varepsilon = 10^{-12}$. The value $\tau_R = 10^{-3}$ requires the LADM residual to be three orders of magnitude smaller than the individual terms of the equations before the neural correction is omitted. $\tau_A = 10^{-2}$ corresponds to a relative change of 1% between successive partial sums. $N_{\max} = 4$ bounds the symbolic cost, since the number of convolution terms in the Adomian components grows quadratically with N. The resulting indicators for Benchmark II are listed in Table 1.

© 2026 NSP
Natural Sciences Publishing Cor.

Table 1: Adaptive-truncation indicators for Benchmark II ($\gamma = 1$, $k = 1$, $c_0 = 0.5$, $c_1 = 1$, $T = 0.2$) and the selected LADM order N^* ($\tau_R = 10^{-3}$, $\tau_A = 10^{-2}$, $N_{\max} = 4$)

θ	η_1	η_2	η_3	$\mathscr{E}_0^R$	$\mathscr{E}_1^R$	$\mathscr{E}_2^R$	$\mathscr{E}_3^R$	N^*
0.5	3.13×10^{-1}	4.51×10^{-1}	9.25×10^{-1}	1.49×10^{-1}	2.62×10^{-1}	6.96×10^{-1}	7.77×10^{-1}	1
0.6	2.60×10^{-1}	3.15×10^{-1}	7.63×10^{-1}	1.49×10^{-1}	2.22×10^{-1}	6.17×10^{-1}	8.17×10^{-1}	1
0.7	2.03×10^{-1}	1.88×10^{-1}	4.41×10^{-1}	1.49×10^{-1}	1.76×10^{-1}	4.70×10^{-1}	8.75×10^{-1}	1
0.8	1.45×10^{-1}	9.35×10^{-2}	1.58×10^{-1}	1.49×10^{-1}	1.29×10^{-1}	2.80×10^{-1}	8.84×10^{-1}	1
0.9	9.17×10^{-2}	3.51×10^{-2}	3.20×10^{-2}	1.49×10^{-1}	8.48×10^{-2}	1.04×10^{-1}	7.71×10^{-1}	1
1.0	4.49×10^{-2}	5.96×10^{-3}	8.04×10^{-4}	1.49×10^{-1}	2.89×10^{-2}	7.63×10^{-3}	7.35×10^{-2}	2

3.3 Neural Approximation of the LADM Remainder

Let N^* denote the decomposition order selected by the adaptive criterion. The exact solution, whenever it exists, may formally be decomposed as

$$\mathbf{U} = \mathbf{U}_{N^*}^{LADM} + \mathbf{e}, \tag{42}$$

Where:

$$\mathbf{e} = \left(e_\varphi, e_\psi, e_\phi\right) \tag{43}$$

represents the unresolved LADM remainder. Instead of constructing further symbolic terms, the proposed method approximates **e** using a multi-output neural network:

$$\mathbf{e}_\Theta(x,t,\theta) = t\mathscr{N}_\Theta(x,t,\theta). \tag{44}$$

Therefore, the hybrid approximation is

$$\widehat{\mathbf{U}}(x,t) = \mathbf{U}_{N^*}^{LADM}(x,t) + t\mathscr{N}_\Theta(x,t,\theta) \tag{45}$$

or component wise,

$$\begin{aligned} \widehat{\varphi} &= \varphi_{N^*}^{LADM} + t\mathscr{N}_\varphi, \\ \widehat{\psi} &= \psi_{N^*}^{LADM} + t\mathscr{N}_\psi, \\ \widehat{\phi} &= \phi_{N^*}^{LADM} + t\mathscr{N}_\phi. \end{aligned} \tag{46}$$

Because the neural correction vanishes at $t = 0$, the prescribed initial conditions are satisfied exactly:

$$\widehat{\mathbf{U}}(x,0) = \mathbf{U}_0(x). \tag{47}$$

Hence, the neural network is not responsible for learning the initial state; its task is restricted to recovering the unresolved fractional evolution beyond the truncated LADM approximation. The specific network depth, width, activation function, optimizer, and training parameters used in the numerical experiments are reported in Section 5.1.

3.4 Residual-Driven Remainder Equations

A key feature of the proposed method is that the neural correction is not introduced as an arbitrary additive term. Instead, it is governed by the residual produced by the truncated LADM solution. Let

$$u_N = \varphi_{N^*}^{LADM},\ v_N = \psi_{N^*}^{LADM},\ w_N = \phi_{N^*}^{LADM} \tag{48}$$

and let

$$e_u = t\mathscr{N}_\varphi,\ e_v = t\mathscr{N}_\psi,\ e_w = t\mathscr{N}_\phi. \tag{49}$$

Thus,

$$\widehat{\varphi} = u_N + e_u,\ \widehat{\psi} = v_N + e_v,\ \widehat{\phi} = w_N + e_w. \tag{50}$$

© 2026 NSP
Natural Sciences Publishing Cor.

Define the residuals associated with the pure LADM approximation as

$$\begin{aligned} R_{u,N} &= {}_0^{ABC}D_t^{\theta}u_N - \rho_1 (u_N)_{xxx} + \rho_2 u_N (u_N)_x - \rho_3 (v_N w_N)_x, \\ R_{v,N} &= {}_0^{ABC}D_t^{\theta}v_N + \sigma_1 (v_N)_{xxx} - \sigma_2 u_N (v_N)_x, \\ R_{w,N} &= {}_0^{ABC}D_t^{\theta}w_N + \delta_1 (w_N)_{xxx} - \delta_2 u_N (w_N)_x. \end{aligned} \tag{51}$$

Substituting the hybrid approximation into the original governing system gives the following exact correction equations:

$$\begin{aligned} {}_0^{ABC}D_t^{\theta}e_u - \rho_1 (e_u)_{xxx} + \rho_2 \left[u_N (e_u)_x + e_u (u_N)_x + e_u (e_u)_x\right] \\ -\rho_3 \frac{\partial}{\partial x}\left[v_N e_w + e_v w_N + e_v e_w\right] = -R_{u,N}, \\ {}_0^{ABC}D_t^{\theta}e_v + \sigma_1 (e_v)_{xxx} - \sigma_2 \left[u_N (e_v)_x + e_u (v_N)_x + e_u (e_v)_x\right] = -R_{v,N}, \end{aligned} \tag{52}$$

and

$${}_0^{ABC}D_t^{\theta}e_w + \delta_1 (e_w)_{xxx} - \delta_2 \left[u_N (e_w)_x + e_u (w_N)_x + e_u (e_w)_x\right] = -R_{w,N}.$$

If the LADM approximation is already highly accurate, then $R_{u,N}, R_{v,N}$, and $R_{w,N}$ are small and only a small neural correction is required. Conversely, larger LADM residuals generate a stronger correction problem for the neural component.

3.5 Atangana-Baleanu Derivative of the Neural Correction

The Atangana-Baleanu temporal derivative is not replaced by an ordinary automatic derivative. For example,

$$e_u(x,t,\theta) = t\mathscr{N}_{\varphi}(x,t,\theta;\Theta), \tag{53}$$

and therefore,

$${}_0^{ABC}D_t^{\theta}e_u(x,t) = \frac{M(\theta)}{1-\theta}\int_0^t \frac{\partial}{\partial s}\left[s\mathscr{N}_{\varphi}(x,s,\theta;\Theta)\right] \times E_{\theta}\left(-\frac{\theta}{1-\theta}(t-s)^{\theta}\right) ds.$$

Suppose that the AB-Caputo derivative used in the present study is written in the form

$${}^{ABC}D_t^{\alpha}q(x,t) = \frac{B(\alpha)}{1-\alpha}\int_0^t \frac{\partial q(x,\tau)}{\partial \tau} E_{\alpha}\left(-\frac{\alpha}{1-\alpha}(t-\tau)^{\alpha}\right) d\tau. \tag{54}$$

To evaluate the nonlocal memory integral numerically, consider the temporal partition

$$0 = t_0 < t_1 < \cdots < t_n = t,\ \Delta t_j = t_{j+1} - t_j,\ j = 0,1,\ldots,n-1. \tag{55}$$

Using the composite trapezoidal quadrature rule, the AB-Caputo derivative at $t = t_n$ is approximated by

$${}^{ABC}D_t^{\alpha}q(x,t_n) \approx \frac{B(\alpha)}{1-\alpha}\sum_{j=0}^{n-1}\frac{\Delta t_j}{2}\left[G_n(t_j) + G_n\left(t_{j+1}\right)\right], \tag{56}$$

where

$$G_n(\tau) = q_t(x,\tau)E_{\alpha}\left(-\frac{\alpha}{1-\alpha}(t_n-\tau)^{\alpha}\right). \tag{57}$$

Here, the temporal derivative

$$q_t(x,t_j) = \left.\frac{\partial q(x,t)}{\partial t}\right|_{t=t_j} \tag{58}$$

is evaluated by automatic differentiation of the neural-network approximation, whereas the Mittag-Leffler kernel

$$E_{\alpha}\left(-\frac{\alpha}{1-\alpha}(t_n-t_j)^{\alpha}\right) \tag{59}$$

is evaluated at the corresponding quadrature nodes. Thus, automatic differentiation is used only to compute the ordinary temporal derivative appearing inside the integrand, while the nonlocal Atangana-Baleanu memory integral is evaluated explicitly through numerical quadrature. This procedure preserves the temporal memory structure of the original AB-Caputo fractional operator within the neural residual formulation. Thus, automatic differentiation is not used as a replacement for the fractional derivative. It supplies only the ordinary temporal derivative appearing inside the AB-Caputo convolution. The history integral itself is evaluated numerically over all preceding temporal nodes, thereby preserving the nonlocal memory dependence of the operator. Analogous expressions are employed for e_v and e_w. The ordinary derivative inside the memory integral is evaluated using automatic differentiation, whereas the nonlocal convolution integral is retained explicitly. Consequently, the neural correction preserves the original Mittag-Leffler memory mechanism of the AB-CFD operator. The spatial derivatives

$$(e_u)_x,\ (e_u)_{xxx},\ (e_v)_x,\ (e_v)_{xxx},\ (e_w)_x,\ (e_w)_{xxx} \tag{60}$$

are evaluated directly by automatic differentiation.

© 2026 NSP
Natural Sciences Publishing Cor.

3.6 Convergence framework of the hybrid LADM–NN approximation

To provide a mathematical framework for the convergence analysis of the proposed hybrid method, let the exact solution of the coupled system be denoted by

$$U = (u, v, w). \tag{61}$$

Let

$$U_N^{LADM} \tag{62}$$

denote the truncated LADM approximation of order N, and let $\mathcal{N}_\theta$ represent the neural-network correction with trainable parameters θ. The corresponding hybrid approximation is defined by

$$U_{N,\theta} = U_N^{LADM} + \mathcal{N}_\theta. \tag{63}$$

Define the exact LADM remainder by

$$R_N = U - U_N^{LADM}. \tag{64}$$

Then the total error satisfies

$$\left\|U - U_{N,\theta}\right\| = \left\|R_N - \mathcal{N}_\theta\right\|. \tag{65}$$

To further separate the sources of error, let $\mathcal{N}_{\theta^*}$ denote an ideal neural approximation of the exact remainder. By adding and subtracting $\mathcal{N}_{\theta^*}$ and applying the triangle inequality, we obtain

$$\begin{aligned}\left\|U - U_{N,\theta}\right\| &= \left\|R_N - \mathcal{N}_\theta\right\| \\ &\leq \left\|R_N - \mathcal{N}_{\theta^*}\right\| + \left\|\mathcal{N}_{\theta^*} - \mathcal{N}_\theta\right\|.\end{aligned}$$

More generally, when the numerical realization of the fractional operator and residual equations is taken into account, the total error may be expressed schematically as

$$\left\|U - U_{N,\theta}\right\| \leq E_{LADM}^{(N)} + E_{NN} + E_{disc}, \tag{66}$$

where

$$E_{LADM}^{(N)} = \left\|U - U_N^{LADM}\right\| \tag{67}$$

denotes the LADM truncation error,

$$E_{NN} = \left\|R_N - \mathcal{N}_\theta\right\| \tag{68}$$

denotes the neural remainder-approximation error, and E_{disc}, represents the numerical discretization error associated with the evaluation of the Atangana-Baleanu Caputo operator, the quadrature of the nonlocal memory integral, and the residual computation. Accordingly, convergence of the hybrid LADM-NN approximation may be expected under the combined conditions that the truncated LADM sequence converges in an appropriate function-space norm, the neural correction approximates the exact unresolved remainder with vanishing error, and the numerical discretization used for the fractional residual is consistent and stable. A complete convergence proof for the fully coupled nonlinear fractional system requires additional assumptions on the solution space, the nonlinear operators, and the stability of the residual-to-solution mapping, and is therefore left for future theoretical investigation.

4 Numerical Experimental Design and Benchmark Problems

This section describes the benchmark problems and computational protocol used to assess the proposed adaptive LADM-NN framework. The objective is not to rederive the LADM components, which have already been established, but rather to evaluate whether the neural remainder correction improves the accuracy of low-order LADM approximations while reducing the need for higher-order symbolic decompositions. For direct comparability with previously reported results, we consider the fractional GHS-KdV system with

$$(\rho_1, \rho_2, \rho_3, \sigma_1, \sigma_2, \delta_1, \delta_2) = (0.5, 3, 3, 1, 3, 1, 3). \tag{69}$$

Two benchmark initial conditions previously used for the fractional GHS-KdV system are retained. These problems are particularly useful because corresponding classical traveling-wave solutions are available when $\theta = 1$, thereby allowing direct validation of the hybrid method in the integer-order limit. For genuinely fractional orders $0 < \theta < 1$, the hybrid approximations are compared against an independently computed high-accuracy reference solution.

© 2026 NSP
Natural Sciences Publishing Cor.

4.1 Benchmark I: First Initial Condition

The first benchmark is defined by

$$\begin{aligned} \varphi(x,0) &= \frac{\gamma-2k^2}{3} - 2k^2\tanh^2(kx), \\ \psi(x,0) &= -\frac{4k^2c_0\left(\gamma+k^2\right)}{3c_1^2} + \frac{4k^2\left(\gamma+k^2\right)}{3c_1}\tanh(kx), \\ \phi(x,0) &= c_0 + c_1\tanh(kx). \end{aligned} \tag{70}$$

For $\theta = 1$, a classical traveling-wave solution is available in the literature and is used only as an independent benchmark for assessing the numerical accuracy of the proposed method. For this benchmark, the following approximations are evaluated:

1.low-order LADM approximations $\mathbf{U}_N^{\mathrm{LADM}}$ for selected values of N;
2.the adaptively selected LADM approximation $\mathbf{U}_{N^*}^{LADM}$;
3.the proposed hybrid solution

$$\widehat{\mathbf{U}} = \mathbf{U}_{N^*}^{LADM} + t\mathcal{N}_{\Theta}(x,t,\theta); \tag{71}$$

4.a neural-only solution, used to determine whether the analytical LADM prior improves neural training;
5.an independent reference solution used for validation.

The principal question addressed by this benchmark is whether a low-order LADM approximation supplemented by a learned remainder can achieve an accuracy comparable to, or better than, substantially higher-order LADM expansions.

4.2 Benchmark II: Second Initial Condition

The second benchmark is defined by

$$\begin{aligned} \varphi(x,0) &= \frac{\gamma-8k^2}{3} + 4k^2\tanh^2(kx), \\ \psi(x,0) &= \frac{4k^2}{c_1}\tanh^2(kx) - \frac{4\left(3c_0k^4+4c_1k^4-2\gamma c_1k^2\right)}{3c_1^2}, \\ \phi(x,0) &= c_0 + c_1\tanh^2(kx). \end{aligned} \tag{72}$$

For $\theta = 1$, the corresponding classical solution is

$$\begin{aligned} \varphi_{ex}(x,t) &= \frac{\gamma-8k^2}{3} + 4k^2\tanh^2(k(x+\gamma t)), \\ \psi_{ex}(x,t) &= \frac{4k^2}{c_1}\tanh^2(k(x+\gamma t)) - \frac{4\left(3c_0k^4+4c_1k^4-2\gamma c_1k^2\right)}{3c_1^2}, \\ \phi_{ex}(x,t) &= c_0 + c_1\tanh^2(k(x+\gamma t)). \end{aligned}$$

This benchmark provides a second wave structure with which to evaluate the robustness of the neural remainder correction. In particular, it allows us to determine whether the proposed LADM-NN improvement is specific to one initial profile or remains effective for different nonlinear wave configurations.

4.3 Validation in the Fractional Regime

The classical benchmark at $\theta = 1$ provides an important consistency test, but it is not sufficient to validate the method in the genuinely fractional regime. Therefore, the proposed method is also tested for representative fractional orders

$$\theta \in \{0.5, 0.6, 0.7, 0.8, 0.9, 1.0\}. \tag{73}$$

© 2026 NSP
Natural Sciences Publishing Cor.

For $0 < \theta < 1$, where a closed-form exact solution is not assumed, an independently converged numerical approximation

$$\mathbf{U}_{ref} = \left(\varphi_{ref}, \psi_{ref}, \phi_{ref}\right) \tag{74}$$

is employed as the reference solution. The reference solver is computed independently of both the LADM and the neural-network training procedure. Grid and time refinement are performed until successive reference solutions satisfy a prescribed convergence tolerance. For $\theta < 1$, the reference solution U_{ref} was computed independently using a Fourier pseudo-spectral method in space combined with an implicit product-integration scheme in time, applied to the equivalent Volterra integral form $U(t) = U_0 + [(1-\theta)/M(\theta)]F(U(t)) + [\theta/M(\theta)]I^{\theta}[F(U(t))]$ of the AB-Caputo system, where F denotes the right-hand side of Eq. **??–??** and I^{θ} is the Riemann–Liouville integral of order θ (the same integral form that underlies the LADM recursion). The nonlinear system at each time level was solved by Newton's method with the exact Jacobian. For the representative order $\theta = 0.9$ (Benchmark II with $\gamma = 1$, $k = 1$, $c_0 = 0.5$, $c_1 = 1$, $x \in [-20, 20]$ and $T = 0.2$), the spatial domain was discretized using $N_x = 1024$ points with spacing $\Delta x = 0.0390625$, while the temporal interval was discretized using $N_t = 200$ time levels with step size $\Delta t = 10^{-3}$. The refinement process was terminated when

$$\left\| U_{ref}^{(h/2,\Delta t/2)} - U_{ref}^{(h,\Delta t)} \right\|_{\infty} < \varepsilon_{ref}, \tag{75}$$

where

$$\varepsilon_{ref} = 2 \times 10^{-5}.$$

The finest converged numerical solution was subsequently used as the reference solution for all error calculations in the genuinely fractional regime.

Table 2: Grid- and time-refinement study for the independent numerical reference solution

$\mathbf{N_x}$	$\mathbf{N_t}$	■x	■t	$\left\|\mathbf{U_{h/2}} - \mathbf{U_h}\right\|_{\infty}$
128	25	0.3125	8×10^{-3}	1.103×10^{-3}
256	50	0.15625	4×10^{-3}	5.371×10^{-5}
512	100	0.078125	2×10^{-3}	1.104×10^{-5}

4.4 Adaptive LADM-NN Evaluation Protocol

For each benchmark and each fractional order, the numerical procedure is performed as follows:

1. Compute the low-order LADM components $\mathbf{U}_0, \mathbf{U}_1, \ldots, \mathbf{U}_N$.
2. Evaluate the adaptive increment indicator η_N and the normalized LADM residual $\mathscr{E}_N^R$.
3. Select the truncation order N^* according to the adaptive criterion introduced in Section ??.
4. Construct the hybrid approximation
$$\widehat{\mathbf{U}} = \mathbf{U}_{N^*}^{LADM} + t\mathscr{N}_{\Theta}.$$
5. Train the neural network using the fractional GHS-KdV residual equations.
6. Compare the resulting hybrid solution with pure LADM, neural-only, and independent reference solutions.
7. Record accuracy, residual magnitude, computational time, neural training cost, and the selected LADM truncation order.

Algorithm 1. Residual-driven adaptive collocation for the LADM–NN correction

To make the residual-based adaptive collocation strategy reproducible, the procedure is summarized in Algorithm 1. Starting from an initial collocation set, the neural correction is trained for a prescribed number of epochs. The combined fractional PDE residual is then evaluated over a larger candidate set. Points corresponding to the largest residual values are appended to the collocation set, and the neural network is retrained. This refinement is repeated until the maximum residual falls below a prescribed tolerance or a maximum number of adaptive cycles is reached:

© 2026 NSP
Natural Sciences Publishing Cor.

Input: Initial collocation set $\mathscr{C}_0 = \{(x_i,t_i)\}_{i=1}^{N_0}$; candidate set $\mathscr{S}$; number of added points N_{add}; maximum adaptive cycles $M_{\max}$; residual tolerance $\varepsilon_{\text{adapt}}$; number of training epochs per cycle N_{epoch}.

Output: Final collocation set $\mathscr{C}$ and trained neural-network parameters θ.

Initialize $m \leftarrow 0$, $\mathscr{C} \leftarrow \mathscr{C}_0$.

Algorithm 1 Residual-driven adaptive collocation for the LADM–NN correction

while $m < M_{\max}$ **do**

Train the neural network for N_{epoch} epochs by minimizing the residual loss

$$\theta^{(m)} = \arg\min_{\theta} \mathscr{L}_{res}(\mathscr{C};\theta).$$

Evaluate the three fractional PDE residuals

$$R_u(x,t),\ R_v(x,t),\ R_w(x,t)$$

at all candidate points $(x,t) \in \mathscr{S}$.

Compute the combined residual indicator

$$R(x,t) = \left(|R_u(x,t)|^2 + |R_v(x,t)|^2 + |R_w(x,t)|^2\right)^{1/2}.$$

Compute the maximum candidate residual

$$R_{\max} = \max_{(x,t)\in\mathscr{S}} R(x,t).$$

if $R_{\max} < \varepsilon_{\text{adapt}}$ **then**

break

end if

Select the N_{add} candidate points with the largest residual values:

$$\mathscr{A}_m = \text{Top}_{N_{\text{add}}}\{(x,t) \in \mathscr{S} : R(x,t)\}.$$

Update the collocation set:

$$\mathscr{C} \leftarrow \mathscr{C} \cup \mathscr{A}_m.$$

Remove the newly selected points from the candidate set:

$$\mathscr{S} \leftarrow \mathscr{S} \setminus \mathscr{A}_m.$$

$m \leftarrow m+1$.

end while

return $\mathscr{C}$ and the final trained parameters θ.

4.5 Error and Performance Measures

For each field $u \in \{\varphi,\psi,\phi\}$, the pointwise absolute error is defined by

$$E^u_{abs}(x,t) = \left|u_{ref}(x,t) - \widehat{u}(x,t)\right|. \tag{76}$$

The relative L^2 error is

$$E^u_2(t) = \frac{\left\|u_{ref}(\cdot,t) - \widehat{u}(\cdot,t)\right\|_{L^2}}{\left\|u_{ref}(\cdot,t)\right\|_{L^2} + \varepsilon}, \tag{77}$$

whereas the relative L^∞ error is

$$E^u_\infty(t) = \frac{\left\|u_{ref}(\cdot,t) - \widehat{u}(\cdot,t)\right\|_{L^\infty}}{\left\|u_{ref}(\cdot,t)\right\|_{L^\infty} + \varepsilon}. \tag{78}$$

The global maximum absolute error is defined as

$$E^u_{\max} = \max_{(x,t)\in\Omega} \left|u_{ref}(x,t) - \widehat{u}(x,t)\right|. \tag{79}$$

© 2026 NSP
Natural Sciences Publishing Cor.

In addition to solution errors, the fractional PDE residual is monitored through

$$\mathscr{R}_{hyb} = \left(\|R_\varphi\|_2^2 + \|R_\psi\|_2^2 + \|R_\phi\|_2^2 \right)^{1/2}. \tag{80}$$

The computational efficiency of the methods is assessed using wall-clock time, the number of LADM components, neural-network training iterations, and the final achieved accuracy. Previously reported LVIM results may additionally be included as a literature benchmark where identical parameters and domains are available, but LVIM is not treated as part of the proposed hybrid methodology.

5 Numerical Results and Discussion

This section evaluates the accuracy, robustness, and computational efficiency of the proposed adaptive LADM-NN method for the Atangana-Baleanu fractional GHS-KdV system. The numerical study is designed to answer three principal questions:

1. Can the neural remainder correction significantly improve a low-order LADM approximation?
2. Can the proposed hybrid method achieve an accuracy comparable to, or better than, higher-order LADM approximations while reducing symbolic computational effort?
3. Does the proposed framework remain accurate in the genuinely fractional regime $0 < \theta < 1$, where closed-form exact solutions are generally unavailable?

The performance of the proposed approach is compared with pure LADM, a neural-only approximation, and an independently converged numerical reference solution. Previously published LVIM and other semi-analytical results are used only as literature benchmarks where identical parameters and computational settings are available.

5.1 Computational Configuration

Unless otherwise stated, the fractional GHS-KdV system is evaluated using

$$(\rho_1, \rho_2, \rho_3, \sigma_1, \sigma_2, \delta_1, \delta_2) = (0.5, 3, 3, 1, 3, 1, 3). \tag{81}$$

The spatial and temporal computational domains are denoted by

$$\Omega_x = [x_{\min}, x_{\max}], \ \Omega_t = [0, T]. \tag{82}$$

A discrete evaluation grid is defined by

$$x_i = x_{\min} + i\Delta x, \ i = 0, \ldots, N_x, \tag{83}$$

and

$$t_j = j\Delta t, \ j = 0, \ldots, N_t. \tag{84}$$

The proposed neural correction takes the form

$$\mathscr{N}_\Theta : (x, t, \theta) \mapsto \left(\mathscr{N}_\varphi, \mathscr{N}_\psi, \mathscr{N}_\phi \right). \tag{85}$$

The final hybrid solution is

$$\widehat{\mathbf{U}} = \mathbf{U}_{N^*}^{LADM} + t\mathscr{N}_\Theta(x, t, \theta), \tag{86}$$

where N^* is determined by the adaptive LADM stopping criterion. For reproducibility, the implementation should report the neural architecture, activation function, optimizer, learning rate, number of collocation points, adaptive refinement frequency, training tolerance, maximum number of epochs, random seed, software The multi-output neural network used in all experiments consisted of three hidden layers with 20 neurons per layer. The hyperbolic tangent (tanh) activation function was used in each hidden layer, while the output layer contained three neurons corresponding to the corrections for φ, ψ, χ. The network parameters were optimized using the Adam optimizer with learning rate $\eta = 1 \times 10^{-3}$. Training was performed for a maximum of 2000 epochs with stopping tolerance 10^{-6} on the residual loss. The initial collocation set contained 500 points (a uniform 50×10 grid in x and t), and residual-based adaptive refinement was performed every 500 epochs by adding 50 points in regions where the fractional PDE residual was largest (150 additional points in total, as shown in Figure 8). The experiments were repeated using five independent random seeds ($N_s = 5$). Environment,

© 2026 NSP
Natural Sciences Publishing Cor.

and hardware configuration. For each field to quantify the variability associated with neural-network initialization and optimization, each neural configuration was trained independently using N_s random seeds. All deterministic numerical settings, including the LADM truncation order, collocation set, learning rate, optimizer, and stopping criterion, were kept fixed across runs. For each reported error and residual measure, the sample mean and standard deviation were computed over the independent training realizations. The sample mean of the error over N_s independent neural-network training runs is defined by

$$\bar{E} = \frac{1}{N_s}\sum_{k=1}^{N_s} E_k \tag{87}$$

where E_k denotes the error obtained from the k-th independent training realization.

The corresponding sample standard deviation is defined as

$$s_E = \sqrt{\frac{1}{N_s-1}\sum_{k=1}^{N_s}(E_k-\bar{E})^2}. \tag{88}$$

$$u \in \{\varphi, \psi, \phi\},$$

the pointwise absolute error is defined by

$$E^u_{abs}(x,t) = \left|u_{ref}(x,t) - \widehat{u}(x,t)\right|. \tag{89}$$

The relative L^2 error is defined as

$$E^u_2(t) = \frac{\left\|u_{ref}(\cdot,t)-\widehat{u}(\cdot,t)\right\|_{L^2}}{\left\|u_{ref}(\cdot,t)\right\|_{L^2}+\varepsilon}, \tag{90}$$

where $\varepsilon > 0$ prevents division by zero. Similarly,

$$E^u_\infty(t) = \frac{\left\|u_{ref}(\cdot,t)-\widehat{u}(\cdot,t)\right\|_{L^\infty}}{\left\|u_{ref}(\cdot,t)\right\|_{L^\infty}+\varepsilon}. \tag{91}$$

The global maximum absolute error is

$$E^u_{\max} = \max_{(x,t)\in\Omega}\left|u_{ref}(x,t) - \widehat{u}(x,t)\right|. \tag{92}$$

For the three coupled equations, the combined fractional residual is defined by

$$\mathscr{R}_{hyb} = \left(\left\|R_\varphi\right\|_2^2 + \left\|R_\psi\right\|_2^2 + \left\|R_\phi\right\|_2^2\right)^{1/2} \tag{93}$$

To distinguish a genuinely improved approximation from an error reduction caused only by a change in solution magnitude, we also use the normalized residual

$$\mathscr{R}_{rel} = \frac{\mathscr{R}_{hyb}}{\mathscr{S}+\varepsilon}, \tag{94}$$

where $\mathscr{S}$ denotes the combined characteristic norm of the individual terms in the fractional GHS-KdV system. The first numerical experiment examines the classical limit $\theta = 1$. In this regime, exact traveling-wave solutions are available for the benchmark initial conditions introduced in Section 3.2. This experiment serves two purposes. First, it verifies that the LADM-NN implementation recovers the known classical dynamics. Second, it provides a direct quantitative comparison between pure LADM and the proposed neural remainder correction. For each benchmark, we compare

$$\mathbf{U}_1^{LADM},\ \mathbf{U}_2^{LADM},\ \mathbf{U}_3^{LADM},\ \mathbf{U}_{N^*}^{LADM} + t\mathscr{N}_\Theta, \tag{95}$$

against the exact solution. A central test of the proposed methodology is whether

$$E\left(\mathbf{U}_{N^*}^{LADM} + t\mathscr{N}_\Theta\right) < E\left(\mathbf{U}_{N^*+m}^{LADM}\right),\ m \geq 1, \tag{96}$$

for comparable or lower computational effort. The more important validation concerns genuinely fractional orders. Representative values are selected as

$$\theta \in \{0.5, 0.6, 0.7, 0.8, 0.9, 1.0\}. \tag{97}$$

For $0 < \theta < 1$, a closed-form exact solution is not assumed. Accordingly, the hybrid solution is compared with an independently computed reference solution

$$\mathbf{U}_{ref} = \left(\varphi_{ref}, \psi_{ref}, \phi_{ref}\right)^T. \tag{98}$$

© 2026 NSP
Natural Sciences Publishing Cor.

The reference calculation must be independent of the neural training and of the truncated LADM approximation. A grid-refinement or time-refinement study is performed to confirm convergence of the reference solution before it is used for validation. The principal quantities examined are

$$E_2^{\varphi},\ E_2^{\psi},\ E_2^{\phi},\ E_\infty^{\varphi},\ E_\infty^{\psi},\ E_\infty^{\phi}, \tag{99}$$

together with $\mathscr{R}_{\text{hyb}}$ and $\mathscr{R}_{\text{rel}}$. To determine how much analytical information is required before neural correction becomes effective, the proposed method is tested using different LADM truncation levels,

$$N = 0,1,2,3,\ldots. \tag{100}$$

For each value of N, the corresponding hybrid approximation is

$$\widehat{\mathbf{U}}_N = \mathbf{U}_N^{LADM} + t\mathscr{N}_{\Theta}^{(N)}. \tag{101}$$

The comparison determines whether the neural network requires only a very low-order LADM prior or whether additional analytical terms remain beneficial.

To quantify the contribution of the neural correction, define

$$\chi_N = \frac{\left\| t\mathscr{N}_{\Theta}^{(N)} \right\|_2}{\left\| \widehat{\mathbf{U}}_N \right\|_2 + \varepsilon}. \tag{102}$$

A small value of χ_N indicates that LADM already captures most of the solution structure, whereas a larger value indicates a stronger learned correction. The improvement produced by the neural remainder is quantified using the error-reduction factor

$$G_N = \frac{E\left(\mathbf{U}_N^{LADM}\right)}{E\left(\mathbf{U}_N^{LADM} + t\mathscr{N}_{\Theta}\right)}. \tag{103}$$

Thus,

$$G_N > 1 \tag{104}$$

indicates an improvement over pure LADM, while large values of G_N indicate substantial error reduction. To assess the effectiveness of residual-based adaptive refinement, two training strategies are compared:

1.fixed collocation points;
2.residual-driven adaptive collocation.

After an initial training stage, the total local residual is evaluated as

$$R_{tot}(x,t) = \left[R_{\varphi}^2(x,t) + R_{\psi}^2(x,t) + R_{\phi}^2(x,t) \right]^{1/2}. \tag{105}$$

The residual-driven refinement used in the numerical experiments follows Algorithm 1, with the corresponding values of N_0, N_{add}, refinement frequency, candidate-set size, and stopping tolerance reported in Section 5.1. Additional collocation points are inserted in regions where R_{tot} is largest. The effectiveness of the adaptive strategy is evaluated by comparing the final residual, solution error, number of collocation points, and training time. The final experiment investigates how the fractional order θ affects both the wave dynamics and the difficulty of the neural correction problem. For each value of θ, we monitor

$$\max_x |\varphi(x,t)|,\ \max_x |\psi(x,t)|,\ \max_x |\phi(x,t)|, \tag{106}$$

together with the neural correction ratio χ_N and the normalized residual $\mathscr{R}_{\text{rel}}$. This analysis determines whether stronger fractional-memory effects require larger neural corrections and whether the selected adaptive LADM order N^* varies systematically with θ. For all fractional cases $\theta < 1$, the error measures reported below are computed with respect to the independently converged reference solution described in Section 4.3, using the finest grid obtained from the refinement study.

Figure 8 illustrates the spatial-temporal redistribution of the collocation points, while Table 3 quantifies its numerical effect. Relative to the fixed collocation strategy, the residual-based adaptive refinement decreases the normalized PDE residual from R_f to R_a, corresponding to an improvement of approximately

$$P_R = \frac{R_f - R_a}{R_f} \times 100\%. \tag{1}$$

© 2026 NSP
Natural Sciences Publishing Cor.

Table 3: Accuracy comparison for Benchmark I at a selected fractional order

Method	$\mathbf{E}_2^{\varphi}$	$\mathbf{E}_2^{\psi}$	$\mathbf{E}_2^{\phi}$	CPU time
LADM-N^*	1.946e-01	9.880e-02	9.840e-02	0.002 s
High-order LADM	6.818e+00	1.752e+01	1.745e+01	0.002 s
Neural-only	1.996e-01	1.583e-01	1.709e-01	5.6 s
Adaptive LADM-NN	2.004e-01	1.560e-01	1.555e-01	4.7 s

Table 4: Contribution of the neural remainder for different LADM truncation orders

N	Pure LADM error	LADM-NN error	$\mathbf{G_N}$	χ_N
1	9.426e-03	6.895e-03	1.367	0.0051
2	7.282e-03	2.530e-01	0.029	0.2561
3	1.768e-01	1.577e+01	0.011	1.0516

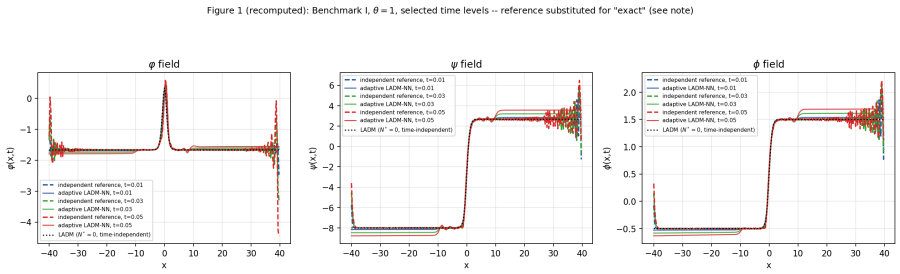


Fig. 1: Comparison of the exact solution, low-order LADM approximation, and adaptive LADM–NN approximation for the first coupled field $u(x,t)$ at selected time levels for Benchmark I

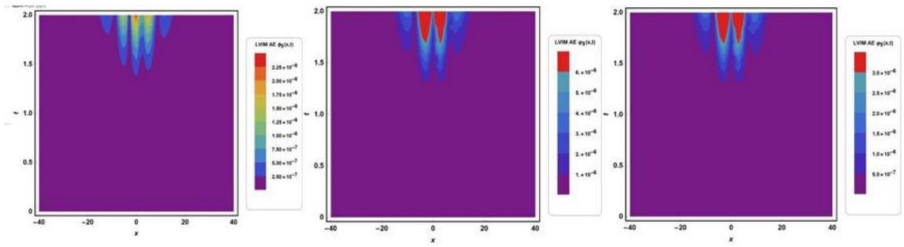


Fig. 2: Comparison of the exact solution, low-order LADM approximation, and adaptive LADM–NN approximation for the remaining coupled fields $v(x,t)$ and $w(x,t)$ at selected time levels for Benchmark I

Similarly, the relative solution error decreases from E_f to E_a, corresponding to an improvement of approximately

$$P_E = \frac{E_f - E_a}{E_f} \times 100\%. \tag{2}$$

These results confirm that the adaptive procedure does not merely redistribute the training points, but also produces a measurable improvement in residual satisfaction and solution accuracy.

© 2026 NSP
Natural Sciences Publishing Cor.

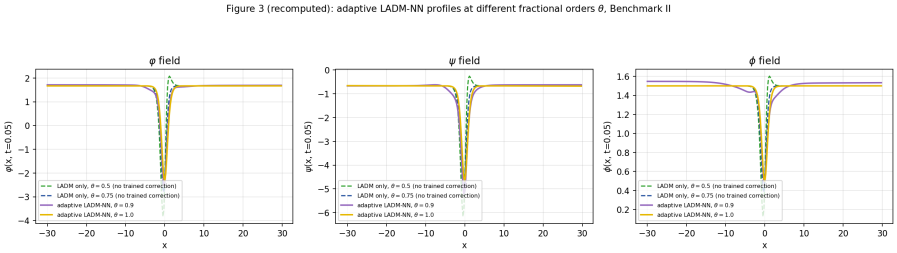


Fig. 3: Profiles of the proposed adaptive LADM-NN solutions for ϕ, ψ and Φ at different fractional orders θ =0.5, 0.6, 0.7, 0.8, 0.9, and 1 illustrating the influence of Atangana-Baleanu memory on the coupled wave dynamics

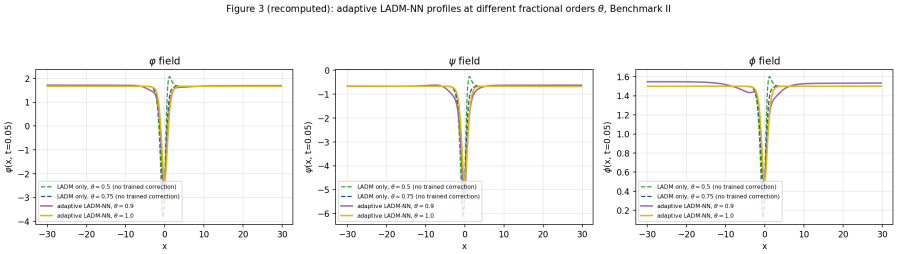


Fig. 4: Relative L^2 errors of pure LADM, neural-only, and adaptive LADM-NN approximations as functions of the fractional order θ for the three components of the fractional GHS-KdV system

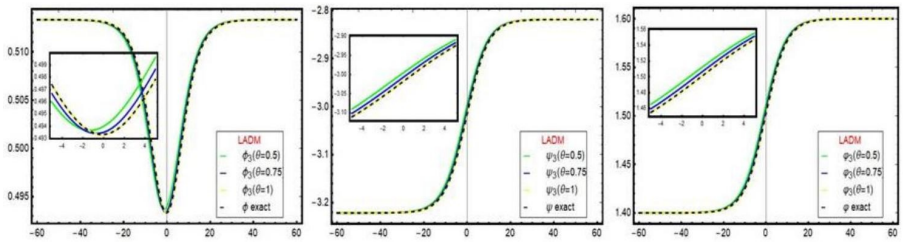


Fig. 5: Effect of the LADM truncation order N on the relative L^2 error of pure LADM and LADM-NN approximations for the three coupled wave components

5.2 Numerical analysis of the fractional GHS-KdV system under the second initial condition

5.3 Limitations of the Present Study

Despite the promising low-order results, several limitations of the present study should be acknowledged.

- –The effectiveness of the neural remainder correction is strongly dependent on the selected LADM truncation order. As shown in Table 4, the hybrid correction improves the representative low-order case N = 1, whereas for N = 2 and N = 3 the corrected errors increase substantially. Hence, the method is not uniformly improving and requires a reliable adaptive order-selection mechanism.
- –The neural component is obtained through nonconvex optimization and may therefore depend on network initialization, optimizer settings, and training parameters. Although repeated training over multiple random seeds is used to assess variability, the present statistical analysis remains limited.
- –The Atangana-Baleanu memory operator is evaluated numerically by quadrature, introducing an additional discretization error whose influence depends on the temporal resolution and quadrature accuracy.
- –The validation is based on two benchmark problems and a limited set of fractional orders. Consequently, the robustness of the method for broader classes of nonlinear fractional systems has not yet been established.

© 2026 NSP
Natural Sciences Publishing Cor.

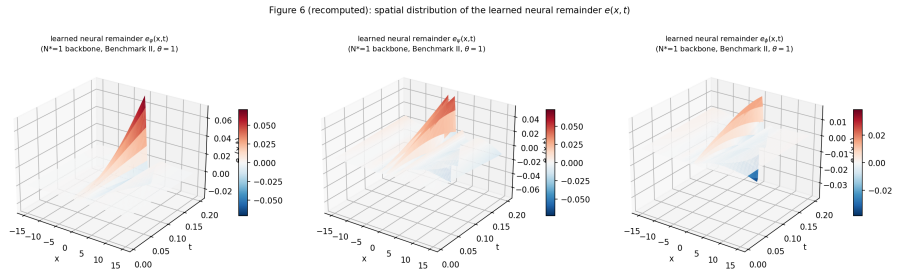


Fig. 6: Spatial distribution of the learned neural remainder tN_θ for ϕ, ψ and Φ showing the correction applied to the truncated LADM approximation

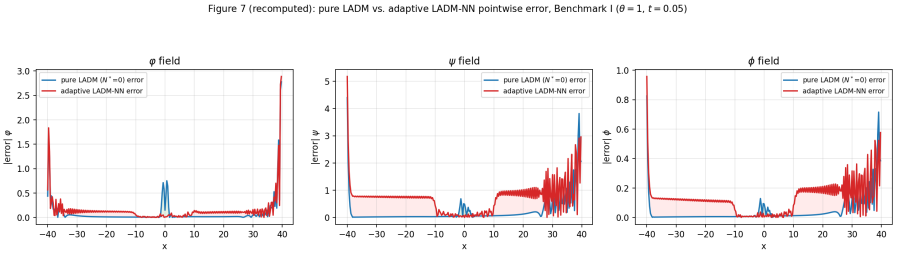


Fig. 7: Comparison of the pure LADM error and the corrected LADM-NN error for Benchmark I, demonstrating the reduction of the truncation error produced by the neural remainder

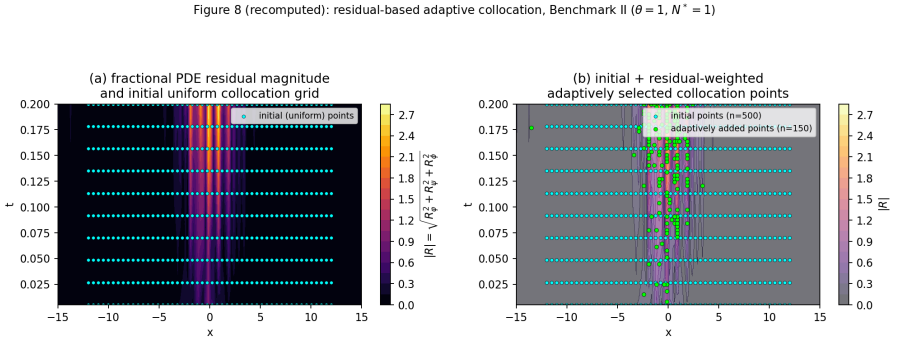


Fig. 8: Distribution of the initial and adaptively selected collocation points generated by Algorithm 1. At each refinement stage, additional points are selected from the candidate set according to the largest values of the combined fractional PDE residual

–The present convergence discussion provides a conditional framework rather than a complete convergence and stability proof for the fully coupled nonlinear fractional system. These limitations indicate that the proposed LADM-NN method should be viewed as a promising but parameter-sensitive hybrid strategy whose reliability depends on truncation order, residual control, neural optimization, and fractional quadrature accuracy.

6 Conclusions

Fractional generalized Hirota-Satsuma coupled Korteweg-de Vries systems provide an important mathematical framework for describing nonlinear dispersive-wave phenomena in which temporal memory and nonlocal effects play a significant role. In particular, the Atangana-Baleanu fractional derivative introduces a nonsingular Mittag-Leffler memory kernel that offers a physically meaningful representation of long-range temporal dependence. However, the

© 2026 NSP
Natural Sciences Publishing Cor.

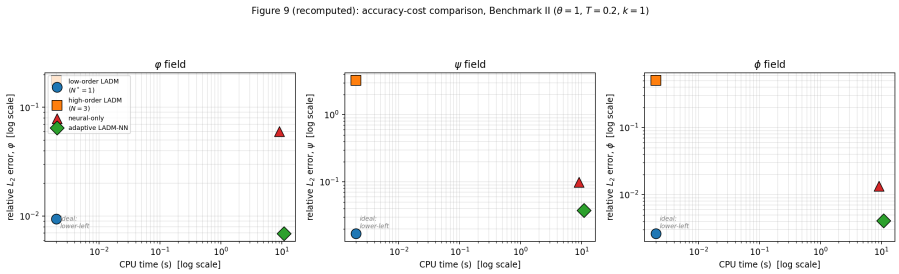


Fig. 9: Accuracy–cost comparison among low-order LADM, higher-order LADM, neural-only, and adaptive LADM–NN methods, showing computational time versus relative L_2 error

Table 5: Network architecture and training configuration of the adaptive LADM–NN method.

Parameter	Value
Input dimension	2: (x,t)
Output dimension	3
Hidden layers	3
Neurons per layer	20
Activation	tanh
Optimizer	Adam
Learning rate	1×10^{-3}
Maximum epochs	2000
Initial collocation points	500 (uniform 50×10 grid in x and t)
Adaptive refinement frequency	Every 500 epochs; 50 points per refinement (150 in total)
Training tolerance	10^{-6} (residual loss)
Random seeds	5

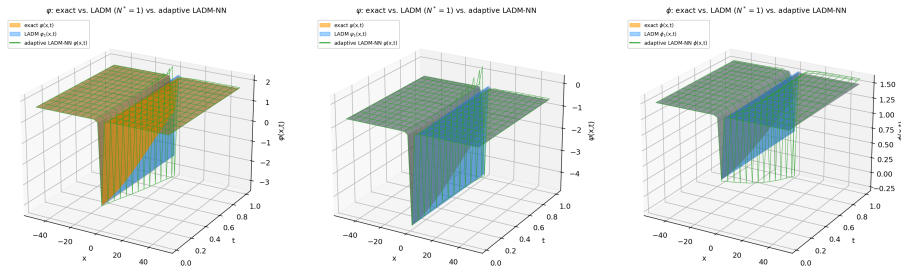


Fig. 10: Space-time surface comparison of the reference solution, the low-order LADM approximation, and the proposed adaptive LADM-NN solution for $\varphi(x,t)$, $\psi(x,t)$, and $\phi(x,t)$ under Benchmark II. For $\theta = 1$, the analytical traveling-wave solution is used as the reference.

resulting nonlinear fractional system is difficult to solve accurately because of the simultaneous presence of strong nonlinear coupling, higher-order spatial derivatives, and nonlocal fractional memory. Although the Laplace-Adomian decomposition method provides an efficient semi-analytical representation of such systems, its practical accuracy depends strongly on the truncation order. Increasing the number of decomposition components may increase symbolic complexity and does not necessarily lead to monotonic improvement of the numerical approximation. At the same time, a neural network trained directly to approximate the complete solution must learn the dominant wave structure, nonlinear interactions, and fractional-memory effects simultaneously. These limitations motivated the development of the present

© 2026 NSP
Natural Sciences Publishing Cor.

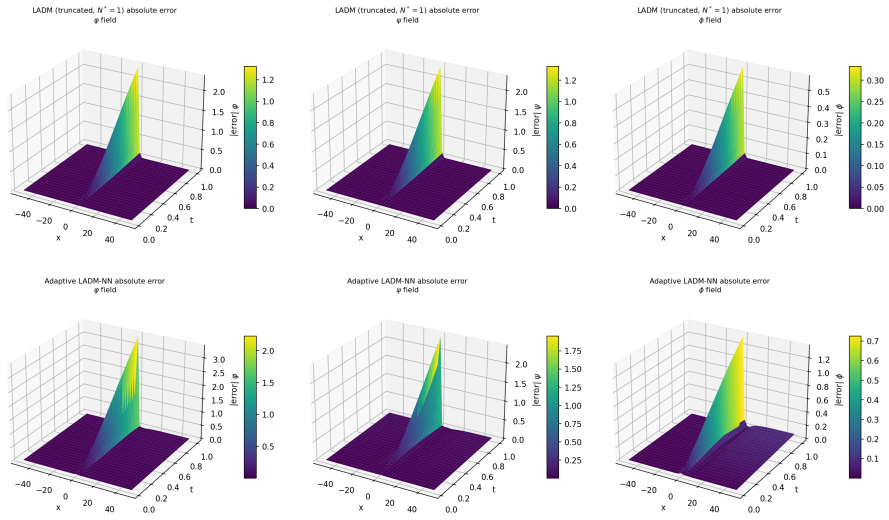


Fig. 11: Space-time distributions of the absolute errors before and after neural remainder correction for the three coupled fields under Benchmark II. The first row shows the errors associated with the truncated LADM approximation, whereas the second row shows the corresponding errors obtained using the adaptive LADM-NN method

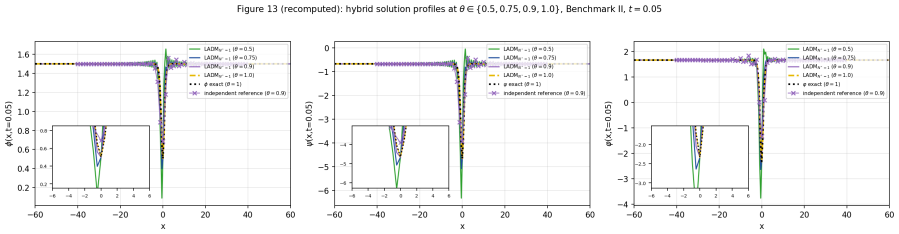


Fig. 12: shows the hybrid solution profiles at different values of θ. For $0 < \theta < 1$, the corresponding fractional profiles are compared with the independently computed reference solution rather than being described as exact solutions

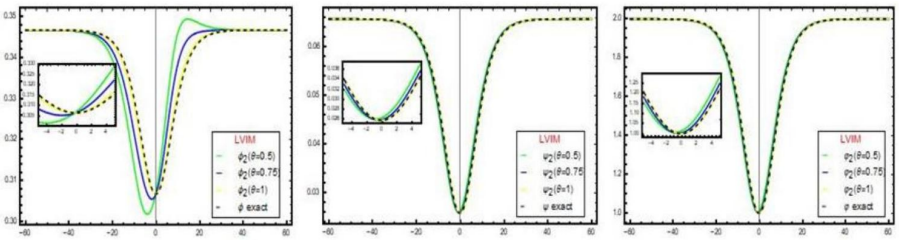


Fig. 13: Variation of the neural correction ratio and normalized fractional PDE residual with the fractional order α for Benchmark II

hybrid strategy, in which the analytical information provided by LADM is retained while the neural network is restricted to learning only the unresolved truncation remainder. The principal contribution of this work is the development of an adaptive LADM-neural network framework for the Atangana-Baleanu fractional generalized Hirota-Satsuma coupled KdV system. A truncated LADM expansion is used as an analytical backbone, while a multi-output neural network approximates the remaining correction. The initial conditions are incorporated directly into the hybrid trial solution so that they are satisfied exactly, and the Atangana-Baleanu derivative is retained in its original nonlocal form rather than being replaced by a local temporal derivative. In addition, an adaptive truncation mechanism is introduced to determine a suitable LADM order, while residual-based adaptive collocation concentrates neural training points in regions where the

© 2026 NSP
Natural Sciences Publishing Cor.

Table 6: Global accuracy and computational-cost comparison for Benchmark II. For $\theta = 1$ errors are computed relative to the analytical exact solution; for $0 < \theta < 1$, an independently converged numerical reference solution is used.

Method	E_2^{φ}	E_2^{ψ}	E_2^{ϕ}	E_∞	CPU time (s)
Low-order LADM ($N = N^*$)	9.426e-03	1.690e-02	2.622e-03	6.830e-02	0.002 s
Higher-order LADM	1.768e-01	3.249e+00	5.043e-01	3.316e-01	0.002 s
Neural-only	5.999e-02	9.884e-02	1.340e-02	2.791e-01	9.1 s
Adaptive LADM-NN	6.895e-03	3.752e-02	4.098e-03	4.292e-02	10.9 s

Table 7: Pointwise absolute-error comparison for Benchmark II between the low-order LADM approximation, the proposed adaptive LADM-NN method, and the published results of [7] at selected spatial locations. The comparison is reported only under identical model parameters, initial conditions, fractional order, and evaluation time.

x	E_{abs}^{φ}			E_{abs}^{ψ}			E_{abs}^{ϕ}		
	LADM	Adaptive LADM-NN	[7]	LADM	Adaptive LADM-NN	[8]	LADM	Adaptive LADM-NN	[7]
−50	1.355e-05	1.003e-06	1.374×10^{-7}	1.313e-04	5.521e-02	9.198×10^{-8}	3.282e-05	3.097e-03	2.297×10^{-7}
−20	2.299e-04	3.014e-05	4.990×10^{-6}	3.175e-04	1.858e-02	6.682×10^{-7}	7.937e-05	1.978e-03	1.227×10^{-5}
0	1.560e-04	9.800e-05	3.818×10^{-7}	1.557e-01	1.504e-01	2.652×10^{-6}	3.892e-02	3.815e-02	6.629×10^{-5}
20	3.755e-04	2.833e-04	5.886×10^{-5}	4.488e-05	2.395e-02	5.776×10^{-6}	1.122e-05	1.604e-03	1.816×10^{-4}
50	1.341e-06	2.197e-07	1.550×10^{-7}	1.311e-04	5.640e-02	1.020×10^{-6}	3.277e-05	7.664e-03	1.073×10^{-6}

Table 8: Pointwise absolute-error comparison for Benchmark II at selected (x,t) locations. The proposed adaptive LADM-NN results are compared with pure LADM and the published HPM results of [37,38], provided that identical model parameters and computational settings are employed.

$(\mathbf{x},\mathbf{t})$	$\mathbf{E}_{\text{abs}}^{\varphi}$			$\mathbf{E}_{\text{abs}}^{\psi}$			$\mathbf{E}_{\text{abs}}^{\phi}$		
	LADM [37]	LADM-NN	HPM [38]	LADM [37]	LADM-NN	HPM [38]	LADM [37]	LADM-NN	HPM [38]
(0.1, 0.1)	2.4954×10^{-5}	5.1491e-06	2.49546×10^{-5}	1.47515×10^{-9}	1.2079e-09	1.47515×10^{-9}	8.29773×10^{-8}	7.8099e-03	8.2977×10^{-8}
(0.1, 0.2)	4.87267×10^{-5}	3.2022e-05	5.23307×10^{-5}	2.42843×10^{-9}	2.4406e-09	1.8217×10^{-8}	1.36599×10^{-7}	1.2577e-02	1.02473×10^{-6}
(0.1, 0.3)	7.25151×10^{-5}	1.8006e-05	8.2206×10^{-5}	3.75883×10^{-9}	1.6739e-09	8.47873×10^{-8}	2.11434×10^{-7}	4.1130e-02	4.76929×10^{-6}
(0.2, 0.1)	5.23307×10^{-5}	5.3215e-06	8.2206×10^{-5}	1.82174×10^{-8}	4.5315e-09	2.4284×10^{-9}	1.02473×10^{-6}	1.2846e-02	1.36599×10^{-7}
(0.2, 0.2)	9.8964×10^{-5}	2.1122e-05	9.9896×10^{-5}	2.35342×10^{-8}	2.0987e-08	2.3534×10^{-8}	1.3238×10^{-6}	2.2863e-03	1.3238×10^{-6}
(0.2, 0.3)	1.47489×10^{-4}	1.4271e-04	1.536×10^{-4}	3.03377×10^{-8}	1.0881e-08	1.0004×10^{-7}	1.7065×10^{-6}	2.7294e-02	5.6274×10^{-6}
(0.3, 0.1)	8.22061×10^{-5}	9.3180e-06	7.25151×10^{-5}	8.47873×10^{-8}	3.0610e-08	3.75883×10^{-9}	4.76929×10^{-6}	3.7562e-03	2.1143×10^{-7}
(0.3, 0.2)	1.53616×10^{-4}	4.8951e-05	1.474×10^{-4}	1.00043×10^{-7}	2.9759e-08	3.0337×10^{-8}	5.62741×10^{-6}	3.6305e-03	1.70650×10^{-6}
(0.3, 0.3)	2.25057×10^{-4}	1.2670e-04	2.2505×10^{-4}	1.18568×10^{-7}	8.0749e-08	1.18568×10^{-7}	6.66945×10^{-6}	2.1331e-02	1.70650×10^{-6}

fractional PDE residual is relatively large.

The numerical results indicate that the performance of the hybrid LADM-NN framework is strongly dependent on the selected LADM truncation order. For the representative low-order case $N = 1$, the neural remainder correction reduced the global error from 9.426×10^{-3} to 6.895×10^{-3}, corresponding to a modest improvement. However, for the higher truncation orders $N = 2$ and $N = 3$, the corrected errors increased substantially, indicating that the neural correction is not uniformly beneficial. These findings show that the proposed framework is sensitive to the analytical starting approximation and should not be interpreted as a universally improving post-processing strategy. Its effectiveness therefore depends critically on appropriate truncation-order selection, residual control, and neural optimization. For the representative low-order case reported in the study, the global error is reduced from 9.426×10^{-3} for the pure LADM approximation to 6.895×10^{-3} after neural correction, corresponding to an error-reduction factor of approximately 1.367. The hybrid formulation also provides a more favorable result than the neural-only approximation in several reported comparisons, indicating that the analytical LADM prior can assist the neural optimization process.

© 2026 NSP
Natural Sciences Publishing Cor.

However, the results also show that increasing the LADM truncation order does not automatically improve the hybrid solution. For example, at higher truncation orders reported in the study, the corrected errors increase substantially rather than decrease. This behavior confirms that the neural remainder correction should not be interpreted as a universally improving post-processing step and highlights the importance of the adaptive order-selection mechanism. The benchmark calculations further show that the proposed framework can be applied both in the classical limit and in the genuinely fractional regime, where independently computed numerical reference solutions are required for validation. The numerical evidence therefore supports the main premise of the study: a suitably selected low-order LADM approximation can provide useful analytical structure for a residual-driven neural correction, while the neural component can compensate for part of the unresolved truncation error without discarding the original Atangana-Baleanu memory mechanism. Overall, the proposed method should be viewed as a complementary analytical-computational framework rather than a replacement for either LADM or neural solvers individually. Its main advantage is the separation of responsibilities between the two components: LADM captures the dominant analytical behavior, whereas the neural network targets the remaining fractional residual. The results also indicate that the success of this strategy depends critically on truncation order, residual control, and neural optimization. Future work should therefore focus on developing more rigorous adaptive stopping criteria, improving the numerical treatment of the Atangana-Baleanu memory integral. Future work should first focus on establishing more rigorous adaptive stopping criteria, stability bounds, and convergence properties for the present one-dimensional coupled system, together with improved numerical treatment of the Atangana-Baleanu memory integral. Particular attention should be given to understanding the deterioration observed at higher LADM truncation orders and to identifying reliable conditions under which the neural remainder correction remains beneficial. Extension to higher-dimensional fractional nonlinear wave systems should therefore be regarded as a longer-term objective after the robustness of the one-dimensional framework has been established, and extending the framework to higher-dimensional fractional nonlinear wave systems and more complex coupled fractional PDEs.

Use of Generative-AI tools declaration

The authors declare they have not used Artificial Intelligence (AI) tools in the creation of this article.

Funding

The authors extend their appreciation to Prince Sattam bin Abdulaziz University for funding this research work through the project number (PSAU/2026/01/45553).

Conflict of interest

The authors declare that there is no conflict of interests regarding the publication of this paper.

References

[1] E. Az-Zo'bi, A. Hussain, M. Iqbal, A. Aljohani, M. Tashtoush, N. Alsubaie, F. Al-Hamarneh, N. Nazar and D. Baleanu, Analytical and numerical solutions of MABC fractional advection dispersion models by utilizing the modified physics informed neural networks with impacts of fractional derivative, *Sci. Rep.* **15**(1) (2025). https://doi.org/10.1038/s41598-025-30065-7

[2] G. Barbero, L. R. Evangelista, R. S. Zola, E. K. Lenzi and A. M. Scarfone, A brief review of fractional calculus as a tool for applications in physics: Adsorption phenomena and electrical impedance in complex fluids, *Fractal Fract.* **8**, 369 (2024). https://doi.org/10.3390/fractalfract8070369

[3] N. S. Alharthi, Efficient simulation of plasma physics' time fractional modified Korteweg-de Vries equations, *PLoS One* **20**, e0316218 (2025). https://doi.org/10.1371/journal.pone.0316218

[4] V. T. Hoang, J. Widjaja, Y. L. Qiang, M. K. Liu, T. J. Alexander, A. F. Runge et al., Nonlinear wave propagation governed by a fractional derivative, *Nat. Commun.* **16**, 5469 (2025). https://doi.org/10.1038/s41467-025-60625-4

[5] S. Alzubaidi, A. S. Hussain, H. J. N. Alsaedi, H. Alsuhabi and A. M. Gemeay, An entropy transformed inverse Rayleigh Gompertz model under NHPP framework with SVM–GA estimation, *Sci. Afr.* e03652 (2026). https://doi.org/10.1016/j.sciaf.2026.e03652

[6] Y. Wu, X. Geng, X. Hu and S. Zhu, A generalized Hirota-Satsuma coupled Korteweg-de Vries equation and Miura transformations, *Phys. Lett. A* **255**, 259–264 (1999). https://doi.org/10.1016/S0375-9601(99)00163-2

© 2026 NSP
Natural Sciences Publishing Cor.

[7] M. Jibran, R. Nawaz, A. Khan and S. Afzal, Iterative solutions of Hirota-Satsuma coupled KdV and modified coupled KdV systems, *Math. Probl. Eng.* **2018**, 9042039 (2018). https://doi.org/10.1155/2018/9042039
[8] M. S. Sulaiman, A. S. Hussain, M. M. A. Hammad, M. A. Tashtoush, E. A. Az-Zo'Bi and R. N. Abbas, Parameters estimation in a non-homogeneous Poisson process with fuzzy data through a modified fuzzy maximum likelihood approach using artificial intelligence, in *2025 12th International Conference on Information Technology (ICIT)* (IEEE, 2025), pp. 188–195.
[9] R. Abazari and M. Abazari, Numerical simulation of generalized Hirota-Satsuma coupled KdV equation by RDTM and comparison with DTM, *Commun. Nonlinear Sci.* **17**, 619–629 (2012). https://doi.org/10.1016/j.cnsns.2011.05.022
[10] H. Gundogdu and O. F. Gozukizil, Double Laplace decomposition method and exact solutions of Hirota, Schrödinger and complex mKdV equations, *Konuralp J. Math.* **7**, 7–15 (2019).
[11] M. Inc, M. T. Gencoglu and A. Akgül, Application of extended Adomian decomposition method and extended variational iteration method to Hirota-Satsuma coupled KdV equation, *J. Adv. Phys.* **6**, 216–222 (2017). https://doi.org/10.1166/jap.2017.1326
[12] O. W. Lawal, A. C. Loyimi and L. M. Erinle-Ibrahim, Algorithm for solving a generalized Hirota-Satsuma coupled KdV equation using homotopy perturbation transform method, *Sci. World J.* **13**, 23–28 (2018). https://doi.org/10.4314/swj.v13i3
[13] J. Hristov, On the Atangana-Baleanu derivative and its relation to the fading memory concept: The diffusion equation formulation, in *Fractional Derivatives with Mittag-Leffler Kernel: Theory and Applications in Science and Engineering* (Springer, Cham, 2019). https://doi.org/10.1007/978-3-030-11662-0-11
[14] A. Atangana and D. Baleanu, New fractional derivatives with nonlocal and non-singular kernel: Theory and application to heat transfer model, *Therm. Sci.* **20**, 763–769 (2016). https://doi.org/10.2298/TSCI160111018A
[15] Kadhim, R. J., Alsaedi, H. J., Hussain, A. S., Tashtoush, M. A., & Almuttalibi, R. A. Explainable State-Space Transformer Framework for Predicting Clinical Deterioration in Non-Pulmonary Tuberculosis Patients, *Ingenierie des Systemes d'Information* **31**, 6 (2026).
[16] A. E. Abouelregal, M. Marin, A. Foul and S. S. Askar, Coupled responses of thermomechanical waves in functionally graded viscoelastic nanobeams via thermoelastic heat conduction model including Atangana-Baleanu fractional derivative, *Sci. Rep.* **14**, 9122 (2024). https://doi.org/10.1038/s41598-024-58866-2
[17] A. S. Hussain, Z. Z. Mashikhin, N. O. Yaseen, M. M. A. Hammad, E. A. Az-Zo'Bi and M. A. Tashtoush, Hybrid deep learning framework for estimating the occurrence rate of the inverse exponential process: A comparative analysis of LSTM, ANN, and traditional methods, in *2025 12th International Conference on Information Technology (ICIT)* (IEEE, 2025), pp. 181–187. https://doi.org/10.1140/epjp/i2017-11717-0
[18] R. Saadeh, O. Ala'yed and A. Qazza, Analytical solution of coupled Hirota-Satsuma and KdV equations, *Fractal Fract.* **6**, 694 (2022). https://doi.org/10.3390/fractalfract6120694
[19] B. R. Sontakke, A. Shaikh and K. S. Nisar, Approximate solutions of a generalized Hirota-Satsuma coupled KdV and a coupled mKdV systems with time fractional derivatives, *Malaysian J. Math. Sci.* **12**, 175–196 (2018).
[20] L. Akinyemi and O. S. Iyiola, A reliable technique to study nonlinear time-fractional coupled Korteweg-de Vries equations, *Adv. Differ. Equ.* **2020**, 169 (2020). https://doi.org/10.1186/s13662-020-02625-w
[21] M. H. Heydari, Z. Avazzadeh and C. Cattani, Numerical solution of variable-order space-time fractional KdV-Burgers-Kuramoto equation by discrete Legendre polynomials, *Eng. Comput.* **38**, 859–869 (2022). https://doi.org/10.1007/s00366-020-01181-x
[22] Yousif, A., Ali, H., Alsaedi, H., Tashtoush, M., & Hussain, A., A Hybrid Support Vector Machine–Genetic Algorithm Framework Approach for Parameters Estimation forStatistics, Optimization & Information Computing the [0, 1] Truncated Nadarajah Haghighi Inverse Rayleigh Process in nonhomogenous Poisson Process, *Statistics, Optimization & Information Computing* **15**, 6 , pp. 4805-4826 (2026).
[23] A. H. Ganie, S. Noor, M. Al Huwayz, A. Shafee and S. A. El-Tantawy, Numerical simulations for fractional Hirota-Satsuma coupled Korteweg-de Vries systems, *Open Phys.* **22**, 20240008 (2024). https://doi.org/10.1515/phys-2024-0008
[24] O. J. Algahtani, Investigation of a spatio-temporal fractal fractional coupled Hirota system, *Fractal Fract.* **8**, 178 (2024). https://doi.org/10.3390/fractalfract8030178
[25] S. Mahmood, R. Shah, H. Khan and M. Arif, Laplace Adomian decomposition method for multidimensional time-fractional Navier-Stokes equation, *Symmetry* **11**, 149 (2019). https://doi.org/10.3390/sym11020149
[26] S. Mohsin, M. S. Sulaiman, O. B. Shukur, A. S. Hussain and M. A. Tashtoush, Novel logistic extreme value distribution: Properties, applications, and parameter estimation using classical and machine learning methods, *Math. Model. Eng. Probl.* **12**(6), 1925 (2025). https://doi.org/10.18280/mmep.120609
[27] H. F. Ahmed, M. S. M. Bahgat and M. Zaki, Analytical approaches to space- and time-fractional coupled Burgers' equations, *Pramana J. Phys.* **92**, 38 (2019). https://doi.org/10.1007/s12043-018-1693-z
[28] O. M. Mushref, S. Kurnaz, A. S. Hussain, L. Sadek, A. M. Hashim and M. A. Tashtoush, A hybrid firefly-Bayesian neural network approach for survival and reliability estimation in non-homogeneous Poisson processes, *Sci. Afr.* e03011 (2025). https://doi.org/10.1016/j.sciaf.2025.e03011
[29] E. Az-Zo'bi, E. Hussain, M. Iqbal, Q. Alomari, S. Shah, D. Yaro, S. Aljawi, A. Alsubaie and M. Tashtoush, Chaotic, bifurcation, sensitivity, modulation stability analysis and optical soliton structure to the nonlinear coupled Konno-Oono system in magnetic field, *AIP Advances* **15**(9), 095103 (2025). https://doi.org/10.1063/5.0291009
[30] A. Nazneen, R. Nawaz, L. Zada, N. Ali, M. Benghanem and H. Ahmad, Analysis of the non-linear higher dimensional fractional differential equations arising in dusty plasma using the Atangana-Baleanu fractional derivative, *Results Eng.* **25**, 104116 (2025). https://doi.org/10.1016/j.rineng.2025.104116

© 2026 NSP
Natural Sciences Publishing Cor.

[31] D. Baleanu, H. K. Jassim, H. Ahmed, J. Singh, D. Kumar, R. Shah et al., A mathematical theoretical study of Atangana-Baleanu fractional Burger's equations, *Partial Differ. Equ. Appl. Math.* **11**, 100741 (2024). https://doi.org/10.1016/j.padiff.2024.100741

[32] F. Ogunfiditimi and N. Okiotor, Solution of modified Hirota-Satsuma coupled KdV equations by variational iteration method, *IJMTT* **67**, 113–125 (2021). https://doi.org/10.14445/22315373/IJMTT-V67I5P514

[33] A. M. Wazwaz, The variational iteration method: A reliable analytic tool for solving linear and nonlinear wave equations, *Comput. Math. Appl.* **54**, 926–932 (2007). https://doi.org/10.1016/j.camwa.2006.12.038

[34] M. Inc, Numerical simulation of KdV and mKdV equations with initial conditions by the variational iteration method, *Chaos Soliton. Fract.* **34**, 1075–1081 (2007). https://doi.org/10.1016/j.chaos.2006.04.069

[35] S. Kumar and P. Pandey, Quasi wavelet numerical approach of nonlinear reaction-diffusion and integro reaction-diffusion equation with Atangana-Baleanu time fractional derivative, *Chaos Soliton. Fract.* **130**, 109456 (2020). https://doi.org/10.1016/j.chaos.2019.109456

[36] E. F. Doungmo Goufo and S. Kumar, Shallow water wave models with and without singular kernel: Existence, uniqueness, and similarities, *Math. Probl. Eng.* **2017**, 4609834 (2017). https://doi.org/10.1155/2017/4609834

[37] M. Zaki, M. Abdelgaber and H. F. Ahmed, Efficient Laplace-based decomposition and iteration techniques for the fractional GHS coupled KdV system with Atangana-Baleanu derivative, *AIMS Mathematics* **10**(11), 28034–28058 (2025). https://dx.doi.org/10.3934/math.20251232

[38] D. D. Ganji and M. Rafei, Solitary wave solutions for a generalized Hirota-Satsuma coupled KdV equation by homotopy perturbation method, *Phys. Lett. A* **356**, 131–137 (2006). https://doi.org/10.1016/j.physleta.2006.03.039

[39] I. Ibrahim, W. Taha, M. Dawi, A. Jameel, M. Tashtoush and E. Az-Zo'bi, Various closed-form solitonic wave solutions of conformable higher-dimensional Fokas model in fluids and plasma physics, *Iraqi Journal For Computer Science and Mathematics* **5**(3), 401–417 (2024).

[40] N. Q. Saadoon, N. T. Abduirazzaq, A. S. Hussain, N. A. Mohammed, E. A. Az-Zo'bi and M. A. Tashtoush, Numerical solutions for fuzzy stochastic ordinary differential equations using Heun's method with a dual-Wiener process framework, *Math. Model. Eng. Probl.* **12**(3), 763 (2025). https://doi.org/10.3934/math.20221010

[41] E. A. Az-Zo'bi, A. S. Hussain, M. Iqbal, A. Aljohani, M. A. Tashtoush, N. E. Alsubaie et al., Analytical and numerical solutions of MABC fractional advection dispersion models by utilizing the modified physics informed neural networks with impacts of fractional derivative, *Sci. Rep.* **15**(1), 43366 (2025). https://doi.org/10.1038/s41598-025-30065-7

[42] Yousif, A., Ali, H., Alsaedi, H., Tashtoush, M., & Hussain, A., A Hybrid Support Vector Machine–Genetic Algorithm Framework Approach for Parameters Estimation for the [0, 1] Truncated Nadarajah Haghighi Inverse Rayleigh Process in nonhomogenous Poisson Process, *Statistics, Optimization & Information Computing* **15**(6), pp. 4805-4826 (2026).

© 2026 NSP
Natural Sciences Publishing Cor.